HOKKAIDO UNIVERSITY

Title	Chaotic motion of the N-vortex problem on a sphere I: Saddle-centers in two-degree-of-freedom
Author(s)	SAKAJO, Takashi; YAGASAKI, Kazuyuki
Citation	Hokkaido University Preprint Series in Mathematics, 858, 1-34
Issue Date	2007-06-06
DOI	https://doi.org/10.14943/84008
Doc URL	https://hdl.handle.net/2115/69667
Type	departmental bulletin paper
File Information	re858.pdf

Hokkaido University Collection of Scholarly and Academic Papers : HUSCAP

Chaotic motion of the N-vortex problem on a sphere I: Saddle-centers in two-degree-of-freedom Hamiltonians

Takashi SAKAJO
Department of Mathematics, Hokkaido University,
Sapporo Hokkaido 060-8610, JAPAN.
E-mail : sakajo@math.sci.hokudai.ac.jp.

Kazuyuki YAGASAKI
Department of Mechanical and Systems Engineering, Gifu University,
Gifu 501-1193, JAPAN
E-mail : yagasaki@gifu-u.ac.jp

June 6, 2007

Abstract

We study the motion of N point vortices with $N \in \mathbb{N}$ on a sphere in the presence of fixed pole vortices, which are governed by a Hamiltonian dynamical system with N degrees of freedom. Special attention is paid to the evolution of their polygonal ring configuration called the *N-ring*, in which they are equally spaced along a line of latitude of the sphere when it is unstable. When the number of the point vortices is $N = 5n$ or $6n$ with $n \in \mathbb{N}$, the system is reduced to a two-degree-of-freedom Hamiltonian with some saddle-center equilibria, one of which corresponds to the unstable N-ring. Utilizing a Melnikov-type method applicable to two-degree-of-freedom Hamiltonian systems with saddle-center equilibria and a numerical method to compute stable and unstable manifolds, we prove numerically that there exist transverse homoclinic orbits to unstable periodic orbits in the neighborhood of the saddle-centers and hence chaotic motions occur. Especially, the evolution of the unstable N-ring is shown to be chaotic.

PACS: 47.32.C-,47.52.+j,47.20.Ky
Keywords: Hamiltonian system, point vortex, flow on sphere, chaos, Melnikov method

1 Introduction

We consider an incompressible and inviscid fluid flow on a sphere, which is often used as a model of planetary flows. Since the vorticity, which is defined as the curl of the velocity field, is conserved along the path of a fluid particle, the point on the sphere with non-zero vorticity evolves as if it were a material point, which is called a *point vortex*. Thus for a given initial non-zero vorticity

region, approximating it with a set of the N point vortices, we can reduce the Euler equations to $2N$-dimensional ordinary differential equations, which are referred to as the *N-vortex problem*. Many references of this subject are found in the book of Newton[15].

Let (Θ_m, Ψ_m) denote the position of the mth point vortex in the spherical coordinates. We assume that all the point vortices have an identical strength, which is fixed to the unity without loss of generality. Then the equations of the N point vortices are given by

$$\dot{\Theta}_m = -\frac{1}{4\pi}\sum_{j\neq m}^{N}\frac{\sin\Theta_j\sin(\Psi_m-\Psi_j)}{1-\cos\Theta_m\cos\Theta_j-\sin\Theta_m\sin\Theta_j\cos(\Psi_m-\Psi_j)}, \tag{1.1}$$

$$\begin{aligned}\dot{\Psi}_m = &-\frac{1}{4\pi\sin\Theta_m}\sum_{j\neq m}^{N}\frac{\cos\Theta_m\sin\Theta_j\cos(\Psi_m-\Psi_j)-\sin\Theta_m\cos\Theta_j}{1-\cos\Theta_m\cos\Theta_j-\sin\Theta_m\sin\Theta_j\cos(\Psi_m-\Psi_j)}\\ &+\frac{\Gamma_1}{4\pi}\frac{1}{1-\cos\Theta_m}-\frac{\Gamma_2}{4\pi}\frac{1}{1+\cos\Theta_m}, \qquad m=1,2,\ldots,N,\end{aligned} \tag{1.2}$$

The last two forcing terms in the equation (1.2) represent the flow fields induced by special point vortices that are fixed at the north and the south poles, whose strengths are denoted by Γ_1 and Γ_2 respectively. They are formally introduced in order to incorporate an effect of rotation of the sphere locally.

Equations (1.1) and (1.2) define a dynamical system in the $2N$-dimensional phase space $\mathbb{P}_N$,

$$\boldsymbol{X} = (\Theta_1,\Theta_2,\ldots,\Theta_N,\Psi_1,\Psi_2,\ldots,\Psi_N) \in \mathbb{P}_N \equiv [0,\pi]^N \times (\mathbb{R}/2\pi\mathbb{Z})^N .$$

Solutions of (1.1) and (1.2) exist globally in time since the self-similar collapse of the identical point vortices never occurs[12]. As we will see in §3, the dynamical system can be rewritten as a Hamiltonian system whose Hamiltonian is represented by

$$\begin{aligned}H = &-\frac{1}{4\pi}\sum_{m=1}^{N}\sum_{m<j}^{N}\log(1-\cos\Theta_m\cos\Theta_j-\sin\Theta_m\sin\Theta_j\cos(\Psi_m-\Psi_j))\\ &-\frac{\Gamma_1}{4\pi}\sum_{m=1}^{N}\log(1-\cos\Theta_m)-\frac{\Gamma_2}{4\pi}\sum_{m=1}^{N}\log(1+\cos\Theta_m)\end{aligned} \tag{1.3}$$

in the X-coordinates (see also [15]). In particular, the Hamiltonian (1.3) is constant along solutions of (1.1) and (1.2). We note that the quantity $I = \sum_{m=1}^{N}\cos\Theta_m$ is also invariant due to the invariance of the Hamiltonian with respect to the rotation around the z-axis.

Here we pay special attention to a polygonal ring configuration of the N point vortices aligned at a line of latitude of the sphere, called *the N-ring*. Such a polygonal alignment of coherent vortex structures often appears in numerical simulations of planetary flows[8, 18, 19], but their interaction is too complicated to track their evolutions for a longer time. While the N-ring is one of the simplest models to approximate the evolution of such coherent structures, it is

a relative equilibrium for (1.1) and (1.2) and its stability has been extensively investigated[3, 4, 13, 20].

A goal of the present study is to describe how the N-ring evolves when it becomes unstable under the influence of the pole vortices. However, it is generally difficult to describe the evolution of the N point vortices for large N, since the dimension of the phase space $\mathbb{P}_N$ becomes quite large. One treatment for this difficulty is to reduce the high-dimensional system to a low-dimensional one, in which orbits are regarded as those embedded in the full system. That is to say, if a chaotic solution were found in the reduced system, it would really exist even in the original non-restricted system.

In the present paper, with the systematic reduction method given in [22], the N-vortex problem on the sphere can be reduced to two-degree-of-freedom Hamiltonian systems for $N = 5n$ and $6n$ with $n \in \mathbb{N}$. In the reduced two-degree-of-freedom Hamiltonian systems, the unstable N-ring acquires a special property; The linear stability analysis [20] shows that the N-ring corresponds to a *saddle-center* equilibrium in some cases when it becomes unstable. That is to say, among the four eigenvalues of the linearized system for the N-ring, the two are real, and the other two are purely imaginary. According to the Lyapunov center theorem [14], there exist a one-parameter family of *unstable* periodic orbits, which may have transverse homoclinic orbits yielding chaotic dynamics [9, 26], around the saddle-center. We show that this type of chaos occurs in the reduced systems, by applying a Melnikov-type techniques for[27] for $N = 6$ and by using a numerical technique of [30] for $N = 5$ as well as $N = 6$ with assistance of a standard computer software called "AUTO" [6].

The Melnikov analysis is a familiar method to prove the existence of transverse homo- or heteroclinic orbits to periodic orbits in time-periodic perturbations of single-degree-of-freedom Hamiltonian systems [9, 26]. It has also been extended in several directions (see, e.g., [11, 24, 25] and references therein) but almost all of such extensions are still limited to perturbations of integrable or partially integrable systems with homo- or heteroclinic orbits. However, in the technique of [27], there is no such a restriction on applicable systems, and instead we just assume that there is a saddle-center equilibrium with a homo- or heteroclinic connection on an invariant plane. In addition, unlike the other Melnikov-type techniques, we do not have to compute an infinite integral but only have to estimate a limit of a function in order to check a criterion for the occurrence of chaos. Owing to these advantages, the method is comparatively easily implemented by numerical means and actually made good use of in the present article.

On the other hand, Champneys and Lord [5] presented a numerical technique to compute homoclinic orbits to periodic orbits in Hamiltonian systems and implemented it for a two-degree-of-freedom system via "AUTO". The technique has been recently extended to homo- and heteroclinic orbits to "general" nonhyperbolic trajectories in [30] and to stable and unstable manifolds of normally hyperbolic invariant manifolds in [31]. We apply the numerical technique of [31] to compute the stable and unstable manifolds of periodic orbits near saddle-centers for $N = 5$ and 6.

The paper consists of seven sections. In the next section, we derive four-

dimensional reduced systems from the N-vortex problem by means of the reduction method proposed in the preceding paper [22, 23]. The reduction is successful when the number of the point vortices has the factor either 5 or 6, i.e. $N = 5n$ or $N = 6n$ with $n \in \mathbb{N}$. In §3 we reformulate the reduced systems by introducing some symplectic transformations so that our numerical techniques given in §4 are applicable. In §4 we review the Melnikov-type technique of [27] and describe our numerical methods to detect transverse homo- or heteroclinic orbits to periodic orbits near saddle-centers. In §5 and §6, we apply these methods to the reduced systems for $N = 6$ and $N = 5$ respectively, and show the existence of chaotic orbits. The final section gives a summary and some discussions.

2 Four-dimensional systems in the N-vortex problem

We reduce the $2N$-dimensional system of (1.1) and (1.2) to four-dimensional systems following the reference [22]. First, we review the results of the linear stability analysis of the N-ring [20, 21]. The N-ring configuration at the line of latitude θ_0 is represented by

$$\Theta_m = \theta_0, \qquad \Psi_m = \frac{2\pi m}{N}, \qquad m = 1, \ldots, N.$$

It is a relative equilibrium for the equations (1.1) and (1.2) with the constant longitudinal velocity $V_0(N)$,

$$V_0(N) = \frac{\Gamma_1 - \Gamma_2}{4\pi \sin^2\theta_0} + \frac{(\Gamma_1 + \Gamma_2 + 2\pi)\cos\theta_0}{4\pi \sin^2\theta_0} - \frac{1}{2N}\frac{\cos\theta_0}{\sin^2\theta_0}.$$

When we perturb the N-ring slightly,

$$\Theta_m(t) = \theta_0 + \epsilon\theta_m(t), \qquad \Psi_m(t) = \frac{2\pi m}{N} + V_0(N)t + \epsilon\varphi_m(t), \qquad |\epsilon| \ll 1, \quad (2.1)$$

the linearized equations for (θ_m, φ_m) are given by

$$\dot{\theta}_m = \frac{1}{4\pi \sin\theta_0} \sum_{j\neq m}^{N} \frac{\varphi_m - \varphi_j}{1 - \cos\frac{2\pi}{N}(m-j)}, \quad (2.2)$$

$$\dot{\varphi}_m = \frac{1}{4\pi \sin^3\theta_0} \sum_{j\neq m}^{N} \frac{\theta_m - \theta_j}{1 - \cos\frac{2\pi}{N}(m-j)} + B_N\theta_m, \quad (2.3)$$

where B_N denotes

$$B_N = -\frac{(\Gamma_1 + \Gamma_2 + N - 1)(1 + \cos^2\theta_0) + 2(\Gamma_1 - \Gamma_2)\cos\theta_0}{4\pi \sin^3\theta_0}. \quad (2.4)$$

Eigenvalues of the linearized equations are represented by $\lambda_m^{\pm} = \pm\sqrt{\xi_m\eta_m}$ for $m = 0, \ldots, N-1$, in which

$$\xi_m = \frac{m(N-m)}{4\pi \sin\theta_0}, \qquad \eta_m = \frac{m(N-m)}{4\pi \sin^3\theta_0} + B_N. \quad (2.5)$$

Thus we have $\lambda_m^{\pm} = \lambda_{N-m}^{\pm}$ for $m = 1, \ldots, N-1$ and $\lambda_0^{\pm} = 0$. Accordingly, the eigenvalues $\lambda_M^{\pm}$ are simple and $\lambda_m^{\pm}$ for $m = 1, \ldots, M-1$ are double when $N = 2M$, while all the eigenvalues $\lambda_m^{\pm}$ for $m = 1, \ldots, M$ are double when $N = 2M+1$. Furthermore, since the eigenvalues satisfy $\left(\lambda_i^{\pm}\right)^2 < \left(\lambda_j^{\pm}\right)^2$ for $1 \leq i < j \leq M$, if $\left(\lambda_k^{\pm}\right)^2 < 0 < \left(\lambda_{k+1}^{\pm}\right)^2$ holds for some $k \in \mathbb{N}$, then the eigenvalues $\lambda_m^{\pm}$ are neutrally stable for $m \leq k$, while λ_m^{+} is unstable for $m > k$. Thus, in other words, the stability of the N-ring agrees with that of the largest eigenvalues $\lambda_M^{\pm}$.

Let the vectors $\boldsymbol{\psi}_m^{\pm}$ and $\boldsymbol{\phi}_m^{\pm}$ be defined by

$$\begin{aligned}
\boldsymbol{\psi}_m^{\pm} &= {}^t\Bigg(\sqrt{\xi_m}, \sqrt{\xi_m}\cos\frac{2\pi}{N}m, \cdots, \sqrt{\xi_m}\cos\frac{2\pi}{N}(N-1)m, \\
&\qquad \pm\sqrt{\eta_m}, \pm\sqrt{\eta_m}\cos\frac{2\pi}{N}m, \cdots, \pm\sqrt{\eta_m}\cos\frac{2\pi}{N}(N-1)m\Bigg), \qquad (2.6) \\
\boldsymbol{\phi}_m^{\pm} &= {}^t\Bigg(0, \sqrt{\xi_m}\sin\frac{2\pi}{N}m, \cdots, \sqrt{\xi_m}\sin\frac{2\pi}{N}(N-1)m, \\
&\qquad 0, \pm\sqrt{\eta_m}\sin\frac{2\pi}{N}m, \cdots, \pm\sqrt{\eta_m}\sin\frac{2\pi}{N}(N-1)m\Bigg), \qquad (2.7)
\end{aligned}$$

for $m = 1, \ldots, M = [N/2]$, in which $[x]$ symbolizes the largest integer less than or equals x. They are the eigenvectors corresponding to the double eigenvalues $\lambda_m^{\pm}$ for $m = 1, \ldots, M-1$. As for the eigenvalues $\lambda_M^{\pm}$, $\boldsymbol{\psi}_M^{\pm}$ are the corresponding eigenvectors for $N = 2M$, while $\boldsymbol{\psi}_M^{\pm}$ and $\boldsymbol{\phi}_M^{\pm}$ are those for $N = 2M+1$. They are available to express the evolution of the N point vortices as a linear basis of the $2N$-dimensional phase space $\mathbb{P}_N$, since the vectors (2.6) and (2.7) are linearly independent. However, the number of the vectors (2.6) and (2.7) is just $2N-2$, so we need to introduce two more vectors $\boldsymbol{\zeta}^{\pm}$, orthogonal to (2.6) and (2.7), for this purpose, which are $\boldsymbol{\zeta}^{\pm} = {}^t(1, \cdots, 1, \pm 1, \cdots, \pm 1)$.

Next, we show how to obtain low-dimensional dynamical systems from (1.1) and (1.2). For a point $(\Theta_1, \cdots, \Theta_N, \Psi_1, \cdots, \Psi_N) \in \mathbb{P}_N$, we define the following two discrete transformations. The first one is the rotation of the N point vortices around the z-axis by the degree $\frac{2\pi}{N}p$, which we call the p-shift transformation σ_p:

$$\begin{array}{lllll}
\sigma_p: & \Theta_m' = \Theta_{N-p+m}, & \Psi_m' = \Psi_{N-p+m} + \frac{2\pi p}{N}, & \text{for} & m = 1, \ldots, p, \\
& \Theta_m' = \Theta_{m-p}, & \Psi_m' = \Psi_{m-p} + \frac{2\pi p}{N}, & \text{for} & m = p+1, \ldots, N.
\end{array} \qquad (2.8)$$

The second one is the pole reversal transformation, which replaces the north pole and the south pole by rotating them around the x-axis by the degree π. The pole reversal transformation for $N = 2M+1$, $\pi_o : (\Theta_m, \Psi_m) \mapsto (\Theta_m', \Psi_m')$, is defined by

$$\begin{array}{lll}
\Theta_1' = \pi - \Theta_1, & \Psi_1' = \Psi_1, & \\
\Theta_m' = \pi - \Theta_{N-m+2}, & \Psi_m' = 2\Psi_1 - \Psi_{N-m+2}, & \text{for } m \neq 1.
\end{array} \qquad (2.9)$$

Similarly, the pole reversal transformation for $N = 2M$, $\pi_e : (\Theta_m, \Psi_m) \mapsto$

(Θ'_m, Ψ'_m), becomes

$$\begin{array}{ll} \Theta'_1 = \pi - \Theta_1, & \Psi'_1 = \Psi_1, \\ \Theta'_m = \pi - \Theta_{N-m+2}, & \Psi'_m = 2\pi + 2\Psi_1 - \Psi_{N-m+2}, \qquad \text{for } m \neq 1. \end{array} \tag{2.10}$$

With these discrete transformations we have the existence of the reduced dynamical systems [22].

Proposition 2.1. *Let $N = pq$, $(p, q \in \mathbb{N})$. If $\sigma_p \boldsymbol{x}(0) = \boldsymbol{x}(0)$ for $\boldsymbol{X} \in \mathbb{P}_N$, then $\sigma_p \boldsymbol{X}(t) = \boldsymbol{X}(t)$ for $t \geq 0$. Furthermore, the $2p$-dimensional linear subspace of $\mathbb{P}_N$,*

$$\boldsymbol{X} = \boldsymbol{X}_0 + \sum_k \left(a_k^+ \boldsymbol{\psi}_{kq}^+ + a_k^- \boldsymbol{\psi}_{kq}^- + b_k^+ \boldsymbol{\phi}_{kq}^+ + b_k^- \boldsymbol{\phi}_{kq}^- \right) + c^+ \boldsymbol{\zeta}^+ + c^- \boldsymbol{\zeta}^-, \quad a_k^\pm, b_k^\pm, c^\pm \in \mathbb{R},$$

is invariant with respect to σ_p, where $\boldsymbol{X}_0 = \left(\theta_0, \theta_0, \ldots, \theta_0, 0, \frac{2\pi}{N}, \ldots, \frac{2\pi}{N}(N-1)\right)$.

The proposition claims that there exists $2p$-dimensional dynamical system for $N = pq$, which is symbolized by $\mathbb{P}_N(\sigma_p)$. The σ_p invariant orbit in $\mathbb{P}_N(\sigma_p)$ satisfies the following relations:

$$\Theta_{kp+m}(t) = \Theta_m(t), \qquad \Psi_{kp+m}(t) = \Psi_m(t) + \frac{2\pi}{q}k, \tag{2.11}$$

for $k = 0, \ldots, q-1$ and $m = 1, \ldots, p$. Note that the reduced system can be obtained for every factor p of N, the N-ring at any latitude θ_0 and any strengths of the pole vortices.

Regarding the pole reversal transformations π_e and π_o, we also have the following invariant dynamical systems.

Proposition 2.2. *Let $N = 2M + 1$ and $\Gamma_1 = \Gamma_2$. Then, if $\pi_o \boldsymbol{X}(0) = \boldsymbol{X}(0)$ for $\boldsymbol{X} \in \mathbb{P}_N$, then $\pi_o \boldsymbol{X}(t) = \boldsymbol{X}(t)$ for $t \geq 0$. Furthermore, the $2M$-dimensional linear subspace of $\mathbb{P}_N$,*

$$\boldsymbol{X} = \boldsymbol{X}_0 + \sum_{k=1}^{M} \left(b_k^+ \boldsymbol{\phi}_k^+ + b_k^- \boldsymbol{\phi}_k^- \right), \qquad b_k^\pm \in \mathbb{R}, \tag{2.12}$$

is invariant with respect to π_o, where

$$\boldsymbol{X}_0 = \left(\frac{\pi}{2}, \ldots, \frac{\pi}{2}, 0, \frac{2\pi}{N}, \ldots, \frac{2\pi M}{N}, -\frac{2\pi M}{N}, \ldots, -\frac{2\pi}{N} \right).$$

Proposition 2.3. *Let $N = 2M$ and $\Gamma_1 = \Gamma_2$. Then, if $\pi_e \boldsymbol{X}(0) = \boldsymbol{X}(0)$ for $\boldsymbol{X} \in \mathbb{P}_N$, then $\pi_e \boldsymbol{X}(t) = \boldsymbol{X}(t)$ for $t \geq 0$. Furthermore, the $2(M-1)$-dimensional linear subspace of $\mathbb{P}_N$,*

$$\boldsymbol{X} = \boldsymbol{X}_0 + \sum_{k=1}^{M-1} \left(b_k^+ \boldsymbol{\phi}_k^+ + b_k^- \boldsymbol{\phi}_k^- \right), \qquad b_k^\pm \in \mathbb{R}, \tag{2.13}$$

is invariant with respect to π_e, where $\boldsymbol{X}_0 = \left(\frac{\pi}{2}, \frac{\pi}{2}, \ldots, \frac{\pi}{2}, 0, \frac{2\pi}{N}, \ldots, \frac{2\pi}{N}(N-1)\right)$.

The π_e and π_o invariant dynamical systems are denoted by $\mathbb{P}_N(\pi_e)$ and $\mathbb{P}_N(\pi_o)$ respectively. Unlike $\mathbb{P}_N(\sigma_p)$, they exist under the additional assumption that the strengths of the pole vortices are identical. Furthermore, the invariant linear spaces (2.12) and (2.13) can be defined only for the N-ring at the equator and their dimensions are different. The π_o invariant orbit keeps the following relations,

$$\Theta_1 = \frac{\pi}{2}, \;\; \Psi_1 = 0, \;\; \Theta_m + \Theta_{N-m+2} = \pi, \;\; \Psi_m + \Psi_{N-m+2} = 0, \;\; \text{for} \;\; m \neq 1. \tag{2.14}$$

Similarly, the π_e invariant orbit holds

$$\Theta_1 = \frac{\pi}{2}, \;\; \Psi_1 = 0, \;\; \Theta_m + \Theta_{N-m+2} = \pi, \;\; \Psi_m + \Psi_{N-m+2} = 2\pi, \;\; \text{for} \;\; m \neq 1. \tag{2.15}$$

As a matter of fact, these relations are equivalent owing to $\Psi_m \in (\mathbb{R}/2\pi\mathbb{Z})$.

Combining the p-shift and the pole reversal transformations, we have more propositions, which are used to obtain four-dimensional systems in the paper.

Proposition 2.4. *Let $N = 2M = pq$, $(p, q \in \mathbb{N})$ and $\Gamma_1 = \Gamma_2$. Then, if $\sigma_p\pi_e \boldsymbol{X}(0) = \boldsymbol{X}(0)$ for $\boldsymbol{X} \in \mathbb{P}_N$, then $\sigma_p\pi_e \boldsymbol{X}(t) = \boldsymbol{X}(t)$ for $t \geq 0$. Furthermore, the set of*

$$\boldsymbol{X} = \boldsymbol{X}_0 + \sum_k \left(b_k^+ \boldsymbol{\phi}_{kq}^+ + b_k^- \boldsymbol{\phi}_{kq}^- \right), \qquad b_k^\pm \in \mathbb{R}, \tag{2.16}$$

is invariant with respect to $\sigma_p\pi_e$, where $\boldsymbol{X}_0$ represents the N-ring at the equator.

Proposition 2.5. *Let $N = 2M + 1 = pq$, $(p, q \in \mathbb{N})$ and $\Gamma_1 = \Gamma_2$. Then, if $\sigma_p\pi_o \boldsymbol{X}(0) = \boldsymbol{X}(0)$ for $\boldsymbol{X} \in \mathbb{P}_N$, then $\sigma_p\pi_o \boldsymbol{X}(t) = \boldsymbol{X}(t)$ for $t \geq 0$. Furthermore, the set of*

$$\boldsymbol{X} = \boldsymbol{X}_0 + \sum_k \left(b_k^+ \boldsymbol{\phi}_{kq}^+ + b_k^- \boldsymbol{\phi}_{kq}^- \right), \qquad b_k^\pm \in \mathbb{R}, \tag{2.17}$$

is invariant with respect to $\sigma_p\pi_o$, where $\boldsymbol{X}_0$ represents the N-ring at the equator.

Now, we derive low-dimensional dynamical systems with the above propositions. For the simplest case, where the dimension of the system is two, it is sufficient to plot the contour lines of the reduced Hamiltonian to investigate the evolution of the unstable N-ring, since it is integrable. The second simplest case is a four-dimensional dynamical system with two degree of freedom, which is no longer integrable. Then, the unstable N-ring possibly exhibits a complex behavior. Among the p-shift invariant systems, it is $\mathbb{P}_N(\sigma_2)$ whose dimension is four, but it is integrable because of the existence of the invariant quantity I. Indeed, $\mathbb{P}_N(\sigma_2)$ has already been investigated by the first author [20], which showed the transition of the global structure of periodic orbits. Regarding $\mathbb{P}_N(\pi_o)$ and $\mathbb{P}_N(\pi_e)$, the four dimensional reduced system exists for $N = 5$ and $N = 6$. They are not integrable, since the invariant I is always zero due to (2.14) and (2.15).

Moreover, the reduced systems $\mathbb{P}_N(\sigma_p\pi_o)$ and $\mathbb{P}_N(\sigma_p\pi_e)$ become four-dimensional only when $N = 5n$ or $N = 6n$, which we are going to confirm in what follows. Suppose that a system is $\sigma_p\pi_e$-invariant. Then, for $N = 2M$, it follows from Proposition 2.3 that the π_e invariant space (2.13) is spanned by $\boldsymbol{\phi}_k^{\pm}$ for $k = 1, \ldots, M-1$. In addition, N should have the factor p, i.e. $N = pn$ for $n > 1$. Then the dimension of the $\sigma_p\pi_e$ invariant system is four, when

$$\left[\frac{M-1}{n}\right] = \left[\frac{1}{n}\left(\frac{pn}{2} - 1\right)\right] = \left[\frac{p}{2} - \frac{1}{n}\right] = 2.$$

Since $[\frac{p}{2} - \frac{1}{n}] \geq 3$ for $p \geq 7$ and less than 2 for $p \leq 4$, we have $p = 5$ and 6. In the similar manner, only $p = 5$ is allowed for $N = 2M + 1$.

Thus the four-dimensional reduced dynamical systems embedded in the N vortex problem are $\mathbb{P}_5(\pi_o)$, $\mathbb{P}_6(\pi_e)$, $\mathbb{P}_N(\sigma_5\pi_e)$, $\mathbb{P}_N(\sigma_5\pi_o)$ and $\mathbb{P}_N(\sigma_6\pi_e)$. According to Propositions 2.4 and 2.5, the linear subspaces of the reduced systems are expressed by the four-dimensional set of

$$\boldsymbol{X} = \boldsymbol{X}_0 + b_1^+\boldsymbol{\phi}_n^+ + b_1^-\boldsymbol{\phi}_n^- + b_2^+\boldsymbol{\phi}_{2n}^+ + b_2^-\boldsymbol{\phi}_{2n}^-,$$

which is the eigenspace corresponding to the eigenvalues $\lambda_n^{\pm}$ and $\lambda_{2n}^{\pm}$. Hence, If $(\lambda_n^{\pm})^2 < 0 < (\lambda_{2n}^{\pm})^2$, the N-ring at the equator becomes a saddle-center equilibrium in the four-dimensional system. Thus the reduced system acquires the situation where the abstract theory of two-degree-of-freedom Hamiltonian with saddle-centers[27] is applicable.

Let us finally note that the two-dimensional $\sigma_3\pi_e$ invariant system $\mathbb{P}_N(\sigma_3\pi_e)$ is embedded in $\mathbb{P}_N(\sigma_6\pi_e)$ due to $N = 6n = 3 \times (2n)$. The coordinates in the phase space is represented by

$$\boldsymbol{X} = \boldsymbol{X}_0 + b_2^+\boldsymbol{\phi}_{2n}^+ + b_2^-\boldsymbol{\phi}_{2n}^-. \tag{2.18}$$

Since the two-dimensional dynamical system is integrable, a contour curve of the reduced Hamiltonian corresponds to an orbit of the restricted N point vortices. Furthermore, since $\boldsymbol{\phi}_{2n}^{\pm}$ spans the eigenspace of $\lambda_{2n}^{\pm}$, the unstable and stable manifolds lie in the phase space (2.18). The two-dimensional system plays a significant role in the application of the Melnikov analysis to Hamiltonian with the saddle-centers for $\mathbb{P}_N(\sigma_6\pi_e)$.

3 Symplectic Formulations

3.1 Equations for $\mathbb{P}_N(\sigma_6\pi_e)$

We reformulate the four-dimensional dynamical systems $\mathbb{P}_N(\sigma_6\pi_e)$. It follows from (2.11) and (2.15) that we have the relations for the $\sigma_6\pi_e$ invariant orbit, which are represented by

$$\begin{aligned}\Theta_1 = \Theta_{6k-5} = \tfrac{\pi}{2}, \quad \Theta_2 = \Theta_{6k-4}, \quad \Theta_3 = \Theta_{6k-3}, \quad \Theta_4 = \Theta_{6k-2} = \tfrac{\pi}{2},\\ \Theta_5 = \Theta_{6k-1}, \quad \Theta_6 = \Theta_{6k}, \quad \Theta_2 + \Theta_6 = \pi, \quad \Theta_3 + \Theta_5 = \pi,\end{aligned} \tag{3.1}$$

and

$$\Psi_{6k-5} = \tfrac{2\pi}{n}(k-1), \quad \Psi_{6k-4} = \Psi_2 + \tfrac{2\pi}{n}(k-1), \quad \Psi_{6k-3} = \Psi_3 + \tfrac{2\pi}{n}(k-1),$$
$$\Psi_{6k-2} = \tfrac{\pi}{n} + \tfrac{2\pi}{n}(k-1), \quad \Psi_{6k-1} = \Psi_5 + \tfrac{2\pi}{n}(k-1), \quad \Psi_{6k} = \Psi_6 + \tfrac{2\pi}{n}(k-1),$$
$$\Psi_2 + \Psi_6 = \tfrac{2\pi}{n}, \quad \Psi_3 + \Psi_5 = \tfrac{2\pi}{n}, \tag{3.2}$$

for $k = 1, \ldots, n$.

Note that the equations (1.1) and (1.2) are written in a symplectic form by using the variables $p_m = \cos\Theta_m$ and $q_m = \Psi_m$ as follows[15].

$$\dot{p}_m = -\frac{\partial H}{\partial q_m}, \qquad \dot{q}_m = \frac{\partial H}{\partial p_m}, \qquad m = 1, \ldots, N. \tag{3.3}$$

Introducing the following generating function $W(P_m, q_m)$,

$$W(P_m, q_m) = P_1 q_1 + \sum_{m=2}^{N} P_m(q_m - q_{m-1}),$$

we define the symplectic transformation $(p_m, q_m) \mapsto (P_m, Q_m)$ by

$$p_N = P_N, \quad p_m = \frac{\partial W}{\partial q_m} = P_m - P_{m+1} \text{ for } m = 1, \ldots, N-1, \tag{3.4}$$

$$Q_1 = q_1, \quad Q_m = \frac{\partial W}{\partial P_m} = q_m - q_{m-1} \text{ for } m = 2, \ldots, N. \tag{3.5}$$

With the new variables (P_m, Q_m), we rewrite the equations for the $\sigma_6\pi_e$ invariant dynamical systems.

First, the relations (3.1) are restated in terms of p_m. For $k = 1, \ldots n$, they are equivalent to

$$p_{6k-5} = p_{6k-2} = 0, \quad p_{6k-4} = p_2, \quad p_{6k-3} = p_3, \quad p_{6k-1} = p_5, \quad p_{6k} = p_6,$$
$$p_{6k-4} + p_{6k} = 0, \quad p_{6k-3} + p_{6k-1} = 0. \tag{3.6}$$

With the new variables P_m, $p_{6k-5} = p_{6k-2} = 0$ yields

$$P_{6k-5} = P_{6k-4}, \qquad P_{6k-2} = P_{6k-1}, \tag{3.7}$$

for $k = 1, \ldots, n$. It follows from $p_{6k-3} + p_{6k-1} = 0$ and (3.7) that we have

$$P_{6k-3} = P_{6k}, \tag{3.8}$$

for $k \leq n$. Noting that $p_{6k-3} + p_{6k-1} = p_{6k+3} + p_{6k-1} = 0$, we also have

$$P_{6k+3} - P_{6k+4} + P_{6k-1} - P_{6k} = 0, \quad \text{for } k < n. \tag{3.9}$$

On the other hand, $p_{6k+4} + p_{6k} = 0$ implies that $P_{6k-4} - P_{6k-3} + P_{6k} - P_{6k+1} = 0$ for $k < n$, which is reduced to $P_{6k-4} = P_{6k+1}$ due to (3.8). For $k = n$, since $p_{6n} = P_{6n}$, we have $P_{6n-4} = 0$. Hence, we have

$$P_1 = P_2 = P_7 = \cdots = P_{6k-5} = P_{6k-4} = P_{6k+1} = \cdots = P_{6n-4} = 0. \tag{3.10}$$

Furthermore, $p_{6k-4}+p_{6k}=p_{6k+2}+p_{6k}=0$ is equivalent to $P_{6k+2}-P_{6k+3}+P_{6k}-P_{6k+1}=0$, which leads to $P_{6k}=P_{6k+3}$ due to (3.10). Substituting it into (3.9), we obtain $P_{6k+4}=P_{6k-1}$. Consequently, we have the following relations of P_m for the $\sigma_6\pi_e$ invariant orbit.

$$\begin{aligned}
&P_1=P_2=P_7=\cdots=P_{6k-5}=P_{6k-4}=P_{6k+1}=\cdots=P_{6n-4}=0,\\
&P_3=P_6=P_9=\cdots=P_{6k-3}=P_{6k}=P_{6k+3}=\cdots=P_{6n-3}=P_{6n},\\
&P_4=P_5=P_{10}=\cdots=P_{6k-2}=P_{6k-1}=P_{6k+4}=\cdots=P_{6n-2}=P_{6n-1}.
\end{aligned} \tag{3.11}$$

Next, we rewrite the relation (3.2) in terms of Q_m. It follows from $\Psi_{6k-5}=\frac{2\pi}{n}(k-1)$ and $\Psi_{6k-4}=\Psi_2+\frac{2\pi}{n}(k-1)$ that we obtain $Q_{6k-4}=\Psi_{6k-5}-\Psi_{6k-4}=\Psi_2=Q_2$. Similarly, we have $Q_{6k-3}=Q_3$, $Q_{6k-2}=Q_4$, $Q_{6k-1}=Q_5$ and $Q_{6k}=Q_6$. The relations $\Psi_2+\Psi_6=\frac{2\pi}{n}$ and $\Psi_3+\Psi_5=\frac{2\pi}{n}$ yield $\Psi_3-\Psi_2+\Psi_5-\Psi_6=0$, equivalently

$$Q_3=Q_6. \tag{3.12}$$

Moreover, the other relations $\Psi_4=\frac{\pi}{n}$ and $\Psi_2+\Psi_6=\frac{2\pi}{n}$ are represented by

$$Q_1+Q_2+Q_3+Q_4=\frac{\pi}{n},\quad 2Q_1+2Q_2+Q_3+Q_4+Q_5+Q_6=\frac{2\pi}{n}. \tag{3.13}$$

Hence, it follows from (3.12) and (3.13) that $Q_4=Q_5$. Consequently, we have the relations of the $\sigma_6\pi_e$ invariant orbit for Q_m.

$$\begin{aligned}
&Q_1=0,\qquad Q_2+Q_3+Q_4=\tfrac{\pi}{n},\\
&Q_3=Q_6=\cdots=Q_{6k-3}=Q_{6k}=\cdots=Q_{6n-3}=Q_{6n},\\
&Q_4=Q_5=\cdots=Q_{6k-2}=Q_{6k-1}=\cdots=Q_{6n-2}=Q_{6n-1}.
\end{aligned} \tag{3.14}$$

The Hamiltonian reduced by the σ_6 invariance with the identical pole vortex points, say $\Gamma_1=\Gamma_2\equiv\Gamma$, is given as follows [22].

$$\begin{aligned}
H &= -\frac{n}{4\pi}\sum_{m=1}^{6}\sum_{m<j}^{6}\sum_{l=0}^{n-1}\log\left(1-\cos\Theta_m\cos\Theta_j-\sin\Theta_m\sin\Theta_j\cos\left(\Psi_m-\Psi_j+\frac{2\pi}{n}l\right)\right)\\
&\quad -\frac{n(n-1)+\Gamma n}{4\pi}\sum_{m=1}^{6}\log(1-\cos^2\Theta_m).
\end{aligned} \tag{3.15}$$

Substituting $\cos\Theta_m=p_m=P_m-P_{m+1}$, $\sin\Theta_m=\sqrt{1-p_m^2}=\sqrt{1-(P_m-P_{m+1})^2}$ and the relations (3.11) and (3.14) into the above Hamiltonian, we obtain the

Hamiltonian $H_n^{(6)}$ for $\mathbb{P}_N(\sigma_6\pi_e)$ with two-degree-of-freedom, which is

$$
\begin{aligned}
&H_n^{(6)}(P_3,P_4,Q_3,Q_4) = \\
&-\frac{n}{2\pi}\sum_{l=0}^{n-1}\log\left(1-\sqrt{1-P_3^2}\cos\left(Q_3+Q_4+\frac{2\pi}{n}l-\frac{\pi}{n}\right)\right) \\
&-\frac{n}{2\pi}\sum_{l=0}^{n-1}\log\left(1-\sqrt{1-(P_3-P_4)^2}\cos\left(Q_4+\frac{2\pi}{n}l-\frac{\pi}{n}\right)\right) \\
&-\frac{n}{2\pi}\sum_{l=0}^{n-1}\log\left(1-\sqrt{1-P_3^2}\cos\left(Q_3+Q_4+\frac{2\pi}{n}l\right)\right) \\
&-\frac{n}{2\pi}\sum_{l=0}^{n-1}\log\left(1-\sqrt{1-(P_3-P_4)^2}\cos\left(Q_4+\frac{2\pi}{n}l\right)\right) \\
&-\frac{n}{2\pi}\sum_{l=0}^{n-1}\log\left(1+P_3(P_3-P_4)-\sqrt{(1-P_3^2)(1-(P_3-P_4)^2)}\cos\left(Q_3+\frac{2\pi}{n}l\right)\right) \\
&-\frac{n}{2\pi}\sum_{l=0}^{n-1}\log\left(1-P_3(P_3-P_4)-\sqrt{(1-P_3^2)(1-(P_3-P_4)^2)}\cos\left(Q_3+2Q_4+\frac{2\pi}{n}l\right)\right) \\
&-\frac{n}{4\pi}\sum_{l=0}^{n-1}\log\left(1+P_3^2-(1-P_3^2)\cos\left(2Q_3+2Q_4+\frac{2\pi}{n}l\right)\right) \\
&-\frac{n}{4\pi}\sum_{l=0}^{n-1}\log\left(1+(P_3-P_4)^2-(1-(P_3-P4)^2)\cos\left(2Q_4+\frac{2\pi}{n}l\right)\right) \\
&-\frac{n(n-1)+\Gamma n}{2\pi}\log(1-P_3^2)\log(1-(P_3-P_4)^2).
\end{aligned}
\tag{3.16}
$$

Note that the Hamiltonian $H_1^{(6)}$ is identical to that for $\mathbb{P}_6(\pi_e)$. As we explain in the previous section, $\mathbb{P}_N(\sigma_6\pi_e)$ contains the two-dimensional invariant system $\mathbb{P}_N(\sigma_3\pi_e)$; in addition to (3.1) and (3.2), the $\sigma_3\pi_e$ invariant orbit satisfies

$$\Theta_1=\Theta_4,\quad \Theta_2=\Theta_5,\quad \Theta_3=\Theta_6,\quad \Theta_2+\Theta_3=\pi,\quad \Psi_2+\Psi_3=\frac{\pi}{n},$$

which are equivalent to

$$P_2=P_4=0,\quad Q_2=Q_4,\quad Q_3+2Q_4=\frac{\pi}{n}. \tag{3.17}$$

Hence, substituting (3.17) into (3.16), we have the reduced Hamiltonian with one-degree-of-freedom for the symplectic variables (P_3,Q_3), say $H_{2n}^{(3)}$. Since $\mathbb{P}_N(\sigma_3\pi_e)$ is integrable, the contour line of $H_{2n}^{(3)}$ represents the $\sigma_3\pi_e$ invariant orbit. Remembering that the phase space of the two-dimensional integrable system is the eigenspace corresponding to the eigenvalues $\lambda_{2n}^{\pm}$ in the saddle direction, we just plot the contour lines to obtain the unstable and the stable manifolds for the unstable N-ring.

3.2 Equations for $\mathbb{P}_N(\sigma_5\pi_e)$ and $\mathbb{P}_N(\sigma_5\pi_o)$

When $N=5n$, there exist the four-dimensional dynamical systems $\mathbb{P}_N(\sigma_5\pi_e)$ for even n, and $\mathbb{P}_N(\sigma_5\pi_o)$ for odd n. The two systems give the same Hamiltonian,

since the relation of π_e invariant orbit (2.15) is equivalent to that of π_o invariant orbit (2.14) due to $\Psi_m \in (\mathbb{R}/2\pi\mathbb{Z})$. The $\sigma_5\pi_e$ and $\sigma_5\pi_o$ invariant orbits satisfy the following relations for $k = 1, \ldots, n$:

$$\Theta_{5k-4} = \frac{\pi}{2}, \quad \Theta_{5k-3} = \Theta_2, \quad \Theta_{5k-2} = \Theta_3, \quad \Theta_{5k-1} = \Theta_4, \quad \Theta_{5k} = \Theta_5,$$
$$\Theta_2 + \Theta_5 = \pi, \quad \Theta_3 + \Theta_4 = \pi,$$

and

$$\Psi_{5k-4} = \frac{2\pi}{n}(k-1), \quad \Psi_{5k-3} = \Psi_2 + \frac{2\pi}{n}(k-1), \quad \Psi_{5k-2} = \Psi_3 + \frac{2\pi}{n}(k-1),$$
$$\Psi_{5k-1} = \Psi_4 + \frac{2\pi}{n}(k-1), \quad \Psi_{5k} = \Psi_5 + \frac{2\pi}{n}(k-1),$$
$$\Psi_2 + \Psi_5 = \frac{2\pi}{n}, \quad \Psi_3 + \Psi_4 = \frac{2\pi}{n}.$$

With the same generating function $W(P_m, q_m)$, we define the symplectic transformation of variables $(p_m, q_m) \mapsto (P_m, Q_m)$. In the similar way in $N = 6n$, we rewrite the relations in terms of (P_m, Q_m), which are given by

$$\begin{aligned}
&P_1 = P_2 = P_6 = \cdots = P_{5k-4} = P_{5k-3} = P_{5k+1} = \cdots = P_{5n-4} = P_{5n-3} = 0,\\
&P_3 = P_5 = P_8 = \cdots = P_{5k-2} = P_{5k} = P_{5k+3} = \cdots = P_{5n-2} = P_{5n}, \quad P_4 = P_{5k-1},\\
&Q_3 = Q_5 = \cdots = Q_{5k-2} = Q_{5k} = \cdots = Q_{5n-2} = Q_{5n}, \quad Q_{5k-1} = Q_4,\\
&Q_{5k-3} = Q_2, \quad Q_{5k-4} = Q_1 = 0, \quad Q_2 + Q_3 + \tfrac{Q_4}{2} = \tfrac{\pi}{n}.
\end{aligned} \tag{3.18}$$

Substitution of the relation (3.18) into the σ_5 invariant Hamiltonian leads to the Hamiltonian $H_n^{(5)}$ for $\mathbb{P}_N(\sigma_5\pi_e)$ and $\mathbb{P}_N(\sigma_5\pi_o)$.

$$\begin{aligned}
&H_n^{(5)}(P_3, P_4, Q_3, Q_4) =\\
&-\frac{n}{2\pi}\sum_{l=0}^{n-1}\log\left(1 - \sqrt{1-P_3^2}\cos\left(Q_3 + \frac{Q_4}{2} + \frac{\pi}{n} + \frac{2\pi}{n}l\right)\right)\\
&-\frac{n}{2\pi}\sum_{l=0}^{n-1}\log\left(1 - \sqrt{1-(P_3-P_4)^2}\cos\left(\frac{Q_4}{2} + \frac{\pi}{n} + \frac{2\pi}{n}l\right)\right)\\
&-\frac{n}{2\pi}\sum_{l=0}^{n-1}\log\left(1 + P_3(P_3-P_4) - \sqrt{(1-P_3^2)(1-(P_3-P_4)^2)}\cos\left(Q_3 + \frac{2\pi}{n}l\right)\right)\\
&-\frac{n}{2\pi}\sum_{l=0}^{n-1}\log\left(1 - P_3(P_3-P_4) - \sqrt{(1-P_3^2)(1-(P_3-P_4)^2)}\cos\left(Q_3 + Q_4 + \frac{2\pi}{n}l\right)\right)\\
&-\frac{n}{4\pi}\sum_{l=0}^{n-1}\log\left(1 + P_3^2 - (1-P_3^2)\cos\left(2Q_3 + Q_4 + \frac{2\pi}{n}l\right)\right)\\
&-\frac{n}{4\pi}\sum_{l=0}^{n-1}\log\left(1 + (P_3-P_4)^2 - (1-(P_3-P_4)^2)\cos\left(Q_4 + \frac{2\pi}{n}l\right)\right)\\
&-\frac{n(n-1)+\Gamma n}{2\pi}\log\left(1-P_3^2\right)\left(1-(P_3-P_4)^2\right).
\end{aligned} \tag{3.19}$$

The Hamiltonian $H_1^{(5)}$ is equivalent to that for $\mathbb{P}_5(\pi_o)$. Unlike $\mathbb{P}_N(\sigma_6\pi_e)$, there is no two-dimensional invariant dynamical system embedded in $\mathbb{P}_N(\sigma_5\pi_e)$ and

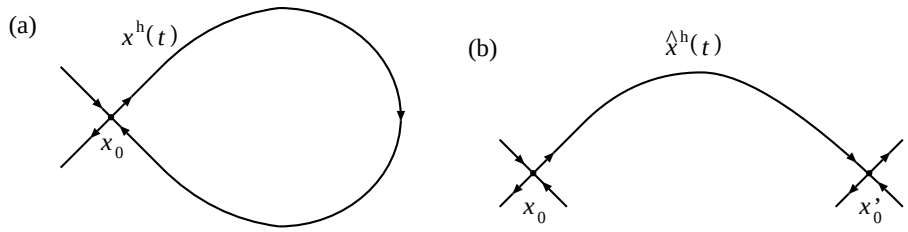

Figure 1: Phase portraits on the $\boldsymbol{x}$-plane: (a) a hyperbolic saddle and a homoclinic orbit; (b) two hyperbolic saddles and a heteroclinic orbit.

$\mathbb{P}_N(\sigma_5\pi_o)$, since the number "5" is prime. It indicates that it is not easy to obtain the unstable and stable manifolds in the saddle direction.

4 Analytical and numerical techniques

In this section we give our analytical and numerical techniques to show that there exist transverse homo- and heteroclinic orbits to periodic orbits near saddle-centers and consequently chaotic dynamics occurs.

4.1 Melnikov-type method

Our analytical technique is the Melnikov-type method of [27] for two-degree-of-freedom Hamiltonian systems with saddle-centers and its extension. We outline the method in our context.

We consider two-degree-of-freedom Hamiltonian systems of the form

$$\dot{\boldsymbol{x}} = J_1 \mathrm{D}_x H(\boldsymbol{x}, \boldsymbol{y}), \quad \dot{\boldsymbol{y}} = J_1 \mathrm{D}_y H(\boldsymbol{x}, \boldsymbol{y}), \quad (\boldsymbol{x}, \boldsymbol{y}) \in \mathbb{R}^2 \times \mathbb{R}^2, \tag{4.1}$$

where $H : \mathbb{R}^2 \times \mathbb{R}^2 \to \mathbb{R}$ is C^{r+1} $(r \geq 3)$ and J_1 is the 2×2 symplectic matrix,

$$J_1 = \begin{pmatrix} 0 & 1 \\ -1 & 0 \end{pmatrix}.$$

We first treat a case in which a saddle-center has a homoclinic orbit in (4.1). More precisely, we make the following assumptions on (4.1).

(A1) The $\boldsymbol{x}$-plane, $\{(\boldsymbol{x}, \boldsymbol{y}) \in \mathbb{R}^2 \times \mathbb{R}^2 \,|\, \boldsymbol{y} = \boldsymbol{0}\}$, is invariant under the flow of (4.1), i.e., $\mathrm{D}_y H(\boldsymbol{x}, \boldsymbol{0}) = \boldsymbol{0}$ for any $\boldsymbol{x} \in \mathbb{R}^2$.

(A2) There is a saddle-center at $(\boldsymbol{x}, \boldsymbol{y}) = (\boldsymbol{x}_0, \boldsymbol{0})$ on the $\boldsymbol{x}$-plane such that the matrix $J_1 \mathrm{D}_x^2 H(\boldsymbol{x}_0, \boldsymbol{0})$ has a pair of real eigenvalues $\pm\lambda$ and the matrix $J_1 \mathrm{D}_y^2 H(\boldsymbol{x}_0, \boldsymbol{0})$ has a pair of purely imaginary eigenvalues $\pm i\omega$ $(\lambda, \omega > 0)$.

Assumption (A2) implies that there exists a one-parameter family of periodic orbits near the saddle-center $(\boldsymbol{x}_0, \boldsymbol{0})$ by the Lyapunov center theorem [14]. In addition, the system restricted on the $\boldsymbol{x}$-plane,

$$\dot{\boldsymbol{x}} = J_1 \mathrm{D}_x H(\boldsymbol{x}, \boldsymbol{0}), \tag{4.2}$$

also has a hyperbolic saddle at $\boldsymbol{x} = \boldsymbol{x}_0$. We also assume the following on (4.2).

(A3) The saddle $\boldsymbol{x} = \boldsymbol{x}_0$ of (4.2) has a homoclinic orbit $\boldsymbol{x}^{\rm h}(t)$. See Fig. 1(a).

Let $\Phi(t)$ and $\Psi(t)$ be fundamental matrices to variational equations in the $\boldsymbol{y}$-direction about the saddle-center $(\boldsymbol{x}_0, \boldsymbol{0})$ and homoclinic orbit $(\boldsymbol{x}, \boldsymbol{y}) = (\boldsymbol{x}^{\rm h}(t), \boldsymbol{0})$, i.e.,

$$\dot{\boldsymbol{\eta}} = J_1 {\rm D}_y^2 H(\boldsymbol{x}_0, \boldsymbol{0})\boldsymbol{\eta} \tag{4.3}$$

and

$$\dot{\boldsymbol{\eta}} = J_1 {\rm D}_y^2 H(\boldsymbol{x}^{\rm h}(t), \boldsymbol{0})\boldsymbol{\eta}, \tag{4.4}$$

respectively, such that $\Phi(0) = I_2$ with I_2 the 2×2 identity matrix. We call (4.4) the *normal variational equation* (NVE) along $\boldsymbol{x}^{\rm h}(t)$. Then the limits

$$B_\pm = \lim_{t \to \pm\infty} \Phi(-t)\Psi(t) \tag{4.5}$$

exist (see Lemma 3.1 of [27] for the proof), and we set $B_0 = B_+ B_-^{-1}$. Define the *Melnikov function* $M(t_0)$ as

$$M(t_0) = m(\boldsymbol{e}_1) - m(B_0 \Phi(t_0)\boldsymbol{e}_1), \tag{4.6}$$

where

$$m(\boldsymbol{\eta}) = \frac{1}{2}\boldsymbol{\eta} \cdot {\rm D}_y^2 H(\boldsymbol{x}_0, \boldsymbol{0})\boldsymbol{\eta}, \tag{4.7}$$

and "$\cdot$" represents the inner product $\boldsymbol{e}_1 = (1, 0)^{\rm T}$ with ${}^{\rm T}$ the transpose operator. Under assumptions (A1)-(A3) we state the result of Theorem 1.1 of [27] as follows.

Theorem 4.1. *Let γ be a periodic orbit sufficiently close to the saddle-center $(\boldsymbol{x}_0, \boldsymbol{0})$. Suppose that $M(t_0)$ has a simple zero, i.e., for some $t_0 = \bar{t}_0$*

$$M(\bar{t}_0) = 0, \quad \frac{\rm d}{{\rm d}t_0} M(\bar{t}_0) \neq 0.$$

Then the stable and unstable manifolds of γ intersect transversely on their energy surface, i.e., transverse homoclinic orbits to γ exist.

The presence of such transverse homoclinic orbits implies that there exists a Smale-horseshoe and hence chaotic dynamics occurs [9, 26].

Next, we consider a case in which two saddle-centers have a heteroclinic orbit in (4.1) and extend Theorem 4.1. In addition to (A1) and (A2), we assume the following.

(A2') There is another saddle-center at $(\boldsymbol{x}, \boldsymbol{y}) = (\boldsymbol{x}_0', \boldsymbol{0})$ with $\boldsymbol{x}_0' \neq \boldsymbol{x}_0$ on the $\boldsymbol{x}$-plane such that the matrix $J_1 {\rm D}_x^2 H(\boldsymbol{x}_0', \boldsymbol{0})$ has a pair of real eigenvalues $\pm\lambda'$ and the matrix $J_1 {\rm D}_y^2 H(\boldsymbol{x}_0', \boldsymbol{0})$ has a pair of purely imaginary eigenvalues $\pm i\omega'$ $(\lambda', \omega' > 0)$.

(A3') The two saddles $\boldsymbol{x} = \boldsymbol{x}_0$ and $\boldsymbol{x}_0'$ in (4.2) are connected by a heteroclinic orbit $\hat{\boldsymbol{x}}^{\rm h}(t)$ such that

$$\lim_{t \to -\infty} \hat{\boldsymbol{x}}^{\rm h}(t) = \boldsymbol{x}_0, \quad \lim_{t \to \infty} \hat{\boldsymbol{x}}^{\rm h}(t) = \boldsymbol{x}_0'.$$

See Fig. 1(b).

Let $\Phi'(t)$ and $\hat{\Psi}(t)$ denote the fundamental matrices for the variational equations in the $\boldsymbol{y}$-direction around the saddle-center $(\boldsymbol{x}_0', \boldsymbol{0})$ and heteroclinic orbit $(\hat{\boldsymbol{x}}^{\mathrm{h}}(t), \boldsymbol{0})$ such that $\Phi'(0) = I_2$. We also show that the limits

$$\hat{B}_- = \lim_{t \to -\infty} \Phi(-t)\hat{\Psi}(t), \quad \hat{B}_+ = \lim_{t \to +\infty} \Phi'(-t)\hat{\Psi}(t) \tag{4.8}$$

exist and set $\hat{B}_0 = \hat{B}_+ \hat{B}_-^{-1}$. Again, define the Melnikov function $\hat{M}(t_0)$ as

$$\hat{M}(t_0) = m(\boldsymbol{e}_1) - m'(\hat{B}_0 \Phi(t_0)\boldsymbol{e}_1), \tag{4.9}$$

where

$$m'(\boldsymbol{\eta}) = \frac{1}{2}\boldsymbol{\eta} \cdot \mathrm{D}_y^2 H(\boldsymbol{x}_0', \boldsymbol{0})\boldsymbol{\eta}. \tag{4.10}$$

Under assumptions (A1), (A2), (A2') and (A3'), modifying arguments in the proof of Theorem 1.1 of [27] slightly, we prove the following result (see Appendix A for the proof).

Theorem 4.2. *Let γ and γ' be periodic orbits sufficiently close to the saddle-centers $(\boldsymbol{x}_0, \boldsymbol{0})$ and $(\boldsymbol{x}_0', \boldsymbol{0})$, respectively, on the same energy surface. Suppose that $\hat{M}(t_0)$ has a simple zero. Then the unstable manifold of γ intersects the stable manifold of γ' transversely on the energy surface, i.e., transverse heteroclinic orbits from γ to γ' exist.*

Exchanging $\boldsymbol{x}_0$ and $\boldsymbol{x}_0'$ and applying Theorem 4.2, we can show that the unstable manifold of γ' intersects the stable manifold of γ transversely on the energy surface. If the statement of the theorem holds in both the situations, then the stable and unstable manifolds of the periodic orbits form a heteroclinic cycle and consequently there exist transverse homoclinic orbits to each periodic orbit [26]. Thus, using Theorem 4.2, we can detect the occurrence of chaos when two saddle-centers have a heteroclinic connection.

As shown in §3, there exists a two-dimensional invariant plane in $\mathbb{P}_N(\sigma_6\pi_e)$ while not in $\mathbb{P}_N(\sigma_5\pi_e)$ and $\mathbb{P}_N(\sigma_5\pi_o)$. Moreover, the invariant plane possesses a saddle-center equilibrium and homo- or heteroclinic orbits for a certain range of Γ, as we see for $\mathbb{P}_6(\pi_e)$ in §5. Hence, some transformation recasts the Hamiltonian system (3.16) into the form (4.1) satisfying assumptions (A1)-(A3) (and (A1), (A2), (A2') and (A3')) for $\mathbb{P}_N(\sigma_6\pi_e)$. Thus, Theorems 4.1 and 4.2 are applicable to $\mathbb{P}_N(\sigma_6\pi_e)$ although it is not to $\mathbb{P}_N(\sigma_5\pi_e)$ and $\mathbb{P}_N(\sigma_5\pi_o)$.

4.2 Numerical computation of criteria for chaos

It is generally difficult to obtain analytical expressions of the homo- and heteroclinic orbits $\boldsymbol{x}^{\mathrm{h}}(t)$ and $\hat{\boldsymbol{x}}^{\mathrm{h}}(t)$ as well as those of the fundamental matrices $\Psi(t)$ and $\hat{\Psi}(t)$ to the variational equations in the $\boldsymbol{y}$-direction, all of which are required to compute the Melnikov functions (4.6) and (4.9). Hence, to estimate the Melnikov functions below, we have to rely on numerical computations including these solutions.

We consider the heteroclinic case: Assumptions (A1), (A2), (A2') and (A3') hold and two saddle-centers $(\boldsymbol{x}, \boldsymbol{y}) = (\boldsymbol{x}_0, \boldsymbol{0})$ and $(\boldsymbol{x}_0', \boldsymbol{0})$ have a heteroclinic orbit

$(\hat{\boldsymbol{x}}^{\mathrm{h}}(t), \mathbf{0})$ Note that we can treat a homoclinic connection in a similar manner if we just set $\boldsymbol{x}_0 = \boldsymbol{x}_0'$. For simplicity, we assume that the matrices $\mathrm{D}_y^2 H(\boldsymbol{x}_0, \mathbf{0})$ and $\mathrm{D}_y^2 H(\boldsymbol{x}_0', \mathbf{0})$ are diagonal. This is the case in $\mathbb{P}_6(\pi_e)$ as seen in §5. We write

$$\mathrm{D}_y^2 H(\boldsymbol{x}_0, \mathbf{0}) = \begin{pmatrix} m_1 & 0 \\ 0 & m_2 \end{pmatrix} \quad \text{and} \quad \mathrm{D}_y^2 H(\boldsymbol{x}_0', \mathbf{0}) = \begin{pmatrix} m_1' & 0 \\ 0 & m_2' \end{pmatrix}. \tag{4.11}$$

The fundamental matrix $\Phi(t)$ is given by

$$\Phi(t) = \begin{pmatrix} \cos \omega t & \sqrt{\dfrac{m_2}{m_1}} \sin \omega t \\ -\sqrt{\dfrac{m_1}{m_2}} \sin \omega t & \cos \omega t \end{pmatrix}, \tag{4.12}$$

where $\omega = \sqrt{m_1 m_2}$. The fundamental matrix $\Phi'(t)$ is also given by (4.12) if ω is replaced with $\omega' = \sqrt{m_1' m_2'}$.

Let $\boldsymbol{v}_1$ and $\boldsymbol{v}_2$ (resp. $\boldsymbol{v}_1'$ and $\boldsymbol{v}_2'$) be (column) eigenvectors for the negative and positive eigenvalues of the Jacobian matrix $J_1 \mathrm{D}_x^2 H(\boldsymbol{x}_0, \mathbf{0})$ (resp. $J_1 \mathrm{D}_x^2 H(\boldsymbol{x}_0', \mathbf{0})$). Then the stable and unstable subspaces E^{s} and E^{u} (resp. E'^{s} and E'^{u}) for $\boldsymbol{x} = \boldsymbol{x}_0$ (resp. for $\boldsymbol{x} = \boldsymbol{x}_0'$) in (4.2) are spanned by $\boldsymbol{v}_1$ and $\boldsymbol{v}_2$ (resp. $\boldsymbol{v}_1'$ and $\boldsymbol{v}_2'$). For $\boldsymbol{x} \in \mathbb{R}^2$, we uniquely determine $\alpha_j, \alpha_j' \in \mathbb{R}$, $j = 1, 2$, such that

$$\boldsymbol{x} = \alpha_1 \boldsymbol{v}_1 + \alpha_2 \boldsymbol{v}_2 = \alpha_1' \boldsymbol{v}_1' + \alpha_2' \boldsymbol{v}_2'. \tag{4.13}$$

Note that $\boldsymbol{x} \in E^{\mathrm{u}}$ or E^{s} if $\alpha_1 = 0$ or $\alpha_2 = 0$ and so on. Let S and S' be 2×2 matrices whose (j,k)-components are given by $\boldsymbol{v}_j \cdot \boldsymbol{v}_k$ and $\boldsymbol{v}_j' \cdot \boldsymbol{v}_k'$, respectively, and let

$$\begin{pmatrix} \boldsymbol{l}_{\mathrm{s}}^{\mathrm{T}} \\ \boldsymbol{l}_{\mathrm{u}}^{\mathrm{T}} \end{pmatrix} = S^{-1} \begin{pmatrix} \boldsymbol{v}_1^{\mathrm{T}} \\ \boldsymbol{v}_2^{\mathrm{T}} \end{pmatrix}, \quad \begin{pmatrix} \boldsymbol{l}_{\mathrm{s}}'^{\mathrm{T}} \\ \boldsymbol{l}_{\mathrm{u}}'^{\mathrm{T}} \end{pmatrix} = S'^{-1} \begin{pmatrix} \boldsymbol{v}_1'^{\mathrm{T}} \\ \boldsymbol{v}_2'^{\mathrm{T}} \end{pmatrix}. \tag{4.14}$$

Since we have $\boldsymbol{x} \cdot \boldsymbol{v}_k = \alpha_1 S_{1k} + \alpha_2 S_{2k} = \alpha_1' S_{1k}' + \alpha_2' S_{2k}'$ for $k = 1, 2$ due to (4.13), we have

$$\begin{pmatrix} \alpha_1 \\ \alpha_2 \end{pmatrix} = \begin{pmatrix} \boldsymbol{l}_{\mathrm{s}}^{\mathrm{T}} \\ \boldsymbol{l}_{\mathrm{u}}^{\mathrm{T}} \end{pmatrix} \boldsymbol{x}, \quad \begin{pmatrix} \alpha_1' \\ \alpha_2' \end{pmatrix} = \begin{pmatrix} \boldsymbol{l}_s'^{\mathrm{T}} \\ \boldsymbol{l}_{\mathrm{u}}'^{\mathrm{T}} \end{pmatrix} \boldsymbol{x}. \tag{4.15}$$

Let $T > 0$ be a sufficiently large constant. We approximate the heteroclinic orbit $\hat{\boldsymbol{x}}^{\mathrm{h}}(t)$ by solving (4.2) numerically under boundary conditions

$$\boldsymbol{l}_s \cdot (\boldsymbol{x}(-T) - \boldsymbol{x}_0) = 0, \quad \boldsymbol{l}_u' \cdot (\boldsymbol{x}(T) - \boldsymbol{x}_0') = 0, \tag{4.16}$$

with $\boldsymbol{x}(-T)$ and $\boldsymbol{x}(T)$ sufficiently close to $\boldsymbol{x}_0$ and $\boldsymbol{x}_0'$, since the stable and unstable manifolds are, respectively, well approximated by the stable and unstable subspaces near $\boldsymbol{x} = \boldsymbol{x}_0$ and $\boldsymbol{x}_0'$. To obtain an approximation of the fundamental matrix $\hat{\Psi}(t)$, we numerically solve the NVE along $\hat{\boldsymbol{x}}^{\mathrm{h}}(t)$ under two initial conditions

$$\boldsymbol{\eta}(-T) = \boldsymbol{e}_1 \quad \text{and} \quad \boldsymbol{\eta}(-T) = \boldsymbol{e}_2, \tag{4.17}$$

where $\boldsymbol{e}_2 = (0, 1)^{\mathrm{T}}$. Finally, using the approximations

$$\hat{B}_- = \Phi(T), \quad \hat{B}_+ = \Phi'(-T)\hat{\Psi}(T), \quad \hat{B}_0 = \Phi'(-T)\hat{\Psi}(T)\Phi(-T), \tag{4.18}$$

we compute (4.9) as follows:

$$\begin{aligned}\hat{M}(t_0) =& \frac{1}{2}m_1 - \frac{1}{2}m_1' \left(\hat{b}_{11}\cos\omega t_0 - \hat{b}_{12}\sqrt{\frac{m_1}{m_2}}\sin\omega t_0\right)^2 \\ & - \frac{1}{2}m_2' \left(\hat{b}_{21}\cos\omega t_0 - \hat{b}_{22}\sqrt{\frac{m_1}{m_2}}\sin\omega t_0\right)^2 \\ =& \frac{1}{2}[(m_1-\beta_0) - \beta_1\cos(2\omega t_0+\tau)], \end{aligned} \tag{4.19}$$

where $\tau \in [0, 2\pi)$ is some constant, $\hat{b}_{jk}$ is the (j,k)-component of the matrix $\hat{B}_0$ and

$$\begin{aligned}\beta_0 &= \frac{1}{2m_2}\left(\hat{b}_{12}^2 m_1 m_1' + \hat{b}_{11}^2 m_2 m_1' + \hat{b}_{22}^2 m_1 m_2' + \hat{b}_{21}^2 m_2 m_2'\right), \\ \beta_1 &= \sqrt{\beta_0^2 - \frac{m_1 m_1' m_2'}{m_2}}.\end{aligned}$$

Here we used the fact that $|\hat{B}_0| = \hat{b}_{11}\hat{b}_{22} - \hat{b}_{12}\hat{b}_{21} = 1$ via the Liouville theorem (e.g., §27 of [2]) for (4.3) and (4.4) since $\mathrm{tr}(J_1 \mathrm{D}_y^2 H(\hat{\boldsymbol{x}}^{\mathrm{h}}(t), \mathbf{0})) = 0$. Hence, if $\beta_1 > |m_1 - \beta_0|$, i.e.,

$$\hat{\Delta} = \hat{b}_{12}^2 m_1 m_1' + \hat{b}_{11}^2 m_2 m_1' + \hat{b}_{22}^2 m_1 m_2' + \hat{b}_{21}^2 m_2 m_2' - m_1 m_2 - m_1' m_2' > 0, \tag{4.20}$$

then the Melnikov function $\hat{M}(t_0)$ has a simple zero and by Theorem 4.2 the unstable manifolds of periodic orbits near $(\boldsymbol{x}_0, \mathbf{0})$ intersect the stable manifolds of periodic orbits near $(\boldsymbol{x}_0', \mathbf{0})$ transversely.

To compute (4.20), we numerically solve (4.2) and (4.4) under the boundary conditions (4.16) and (4.17), respectively, and calculate the matrix $\hat{B}$ by (4.18). Numerical solutions of the boundary value problem along with estimates of $\hat{B}$ and $\hat{\Delta}$ are easily continued with the parameter Γ by the numerical continuation tool "AUTO97" [6], if once a solution is obtained for a special value of Γ. To obtain the *starting solution*, we take a point that is very close to $\boldsymbol{x}_0$ and satisfies the first equation of (4.16) as $\boldsymbol{x}(-T)$, and solve (4.2) and (4.17) as an initial value problem using an adequate numerical method. (See §5 for more details on our concrete approach.)

For the case of the homoclinic orbit $\boldsymbol{x}^{\mathrm{h}}(t)$, setting $\boldsymbol{x}_0' = \boldsymbol{x}_0$ and applying the same argument, we see that if

$$\Delta = b_{12}^2 m_1^2 + (b_{11}^2 + b_{22}^2) m_1 m_2 + b_{21}^2 m_2^2 - 2m_1 m_2 > 0, \tag{4.21}$$

where b_{jk} is the (j,k)-component of the matrix B_0, then $M(t_0)$ has a simple zero and by Theorem 4.1 the stable and unstable manifolds of periodic orbits near $(\boldsymbol{x}_0, \mathbf{0})$ intersect transversely. We also use "AUTO97" to compute the criterion (4.21) in §5.

4.3 Numerical computation of stable and unstable manifolds

As stated in §4.1, the Melnikov approach can not be applied to $\mathbb{P}_N(\sigma_5\pi_e)$ and $\mathbb{P}_N(\sigma_5\pi_e)$ since they contain no invariant plane. However, even in those cases,

we can compute the stable and unstable manifolds of periodic orbits near saddle-centers by the numerical method of [30]. Using this approach, we show that the stable and unstable manifolds intersect transversely and chaotic dynamics occurs for $\mathbb{P}_6(\pi_e)$ and $\mathbb{P}_5(\pi_o)$ n §§5 and 6. We briefly review the numerical method in our context.

Rewrite the Hamiltonian systems for $\mathbb{P}_5(\pi_o)$ and $\mathbb{P}_6(\pi_e)$ as

$$\dot{\boldsymbol{z}} = J_2 \mathrm{D}H(\boldsymbol{z}), \tag{4.22}$$

where $z = (Q_3, Q_4, P_3, P_4)$ or (x_1, y_1, x_2, y_2), $H : \mathbb{R}^4 \to \mathbb{R}$ is the Hamiltonian function and J_2 is the 4×4 symplectic matrix,

$$J_2 = \begin{pmatrix} 0 & I_2 \\ -I_2 & 0 \end{pmatrix}.$$

Recall that I_2 denotes the 2×2 identity matrix.

As in [5], to compute a periodic orbit $\boldsymbol{z} = \bar{\boldsymbol{z}}(t)$ near the saddle-center $\boldsymbol{z} = \boldsymbol{z}_{\mathrm{sc}}$, we solve (4.22) under the periodic boundary condition

$$\bar{\boldsymbol{z}}(0) = \bar{\boldsymbol{z}}(\bar{T}), \tag{4.23}$$

with $\bar{T}$ the period of the periodic orbit, while its phase is fixed at

$$\bar{z}_4(0) = z_{40}, \tag{4.24}$$

with z_j the j-th component of z, and the Hamiltonian constrained to be constant

$$H(\bar{\boldsymbol{z}}(0)) = h, \tag{4.25}$$

where $\bar{T}$ is the period of the periodic orbit. We compute a trajectory $\boldsymbol{z} = \boldsymbol{z}^{\mathrm{u}}(t)$ on the unstable manifold of the periodic orbit $\bar{\boldsymbol{z}}(t)$ by solving (4.22) under the boundary conditions

$$\boldsymbol{z}^{\mathrm{u}}(0) - \bar{\boldsymbol{z}}(0) = \epsilon_{\mathrm{u}} \boldsymbol{e}^{\mathrm{u}}, \quad \boldsymbol{z}^{\mathrm{u}}(T_{\mathrm{u}}) = \boldsymbol{z}_0^{\mathrm{u}}, \tag{4.26}$$

where $\boldsymbol{e}^{\mathrm{u}} \in \mathbb{R}^4$ is an unstable eigenvector with unit modulus of the monodromy matrix for $\bar{\boldsymbol{z}}(t)$, $\epsilon_u \ll 1$ and T_u are positive constants, and $\boldsymbol{z}_0^{\mathrm{u}} \in \mathbb{R}^4$ is a constant vector and represents an approximate point on the unstable manifold. Thus, numerical continuation of the solutions $\bar{\boldsymbol{z}}(t)$ and $\boldsymbol{z}^{\mathrm{u}}(t)$ for the boundary value problem (4.22)-(4.26) gives the unstable manifold. Similarly, we compute the stable manifold by continuing the solution $\bar{\boldsymbol{z}}(t)$ of (4.22) satisfying (4.23)-(4.25) and a solution $\boldsymbol{z}^{\mathrm{s}}(t)$ of (4.22) satisfying the boundary conditions

$$\boldsymbol{z}^{\mathrm{s}}(0) - \bar{\boldsymbol{z}}(0) = \epsilon_{\mathrm{s}} \boldsymbol{e}^{\mathrm{s}}, \quad \boldsymbol{z}^{\mathrm{s}}(-T_{\mathrm{s}}) = \boldsymbol{z}_0^{\mathrm{s}}, \tag{4.27}$$

where $\boldsymbol{e}^{\mathrm{s}} \in \mathbb{R}^4$ is a stable eigenvector with unit modulus of the monodromy matrix for $\bar{\boldsymbol{z}}(t)$, $\epsilon_s \ll 1$ and T_s are positive constants, and a constant vector $\boldsymbol{z}_0^{\mathrm{s}} \in \mathbb{R}^4$ represents an approximate point on the stable manifold. In the continuations $\bar{T}$, $T_{\mathrm{u,s}}$, $\epsilon_{\mathrm{u,s}}$, z_{40} or $\boldsymbol{z}_0^{\mathrm{u,s}}$ are taken as the free parameters.

In the numerical computations of §§5 and 6, we make a small modification in the standard version of "AUTO97" so that the monodromy matrices of periodic

orbits are provided at each step in the computation, as in [5]. Without the modification, we have to solve the 4×4 matrix version of the four-dimensional, linearized system of (4.25) around the periodic orbits to obtain the monodromy matrices. Owing to this modification, the dimension of the system to be solved is decreased by 16, so that we just solve an eight-dimensional system to compute the periodic orbits and orbits on its stable or unstable manifolds. As the starting solutions for the continuations by "AUTO97", we take solutions of the linearized system

$$\dot{\boldsymbol{\zeta}} = J_2 \mathrm{D}^2 H(\boldsymbol{z}_{\mathrm{sc}})\boldsymbol{\zeta}, \tag{4.28}$$

with the following forms:

$$\bar{\boldsymbol{z}}(t) = \boldsymbol{z}_{\mathrm{sc}} + \epsilon_c(\boldsymbol{e}_0^{+c} e^{i\omega t} + \boldsymbol{e}_0^{-c} e^{-i\omega t}), \quad t \in [0, \bar{T}], \tag{4.29}$$

and

$$\boldsymbol{z}^{\mathrm{u}}(t) = \bar{\boldsymbol{z}}(t) + \epsilon_{\mathrm{u}} \boldsymbol{e}_0^{\mathrm{u}} e^{\lambda_{\mathrm{u}} t}, \quad t \in [0, T_u], \tag{4.30}$$

or

$$\boldsymbol{z}^{\mathrm{s}}(t) = \bar{\boldsymbol{z}}(t) + \epsilon_{\mathrm{s}} \boldsymbol{e}_0^{\mathrm{s}} e^{\lambda_{\mathrm{s}} t}, \quad t \in [-T_{\mathrm{s}}, 0], \tag{4.31}$$

where λ_s, λ_u and $\pm i\omega$ are the stable, unstable and center eigenvalues of $J_2 \mathrm{D}^2 H(\boldsymbol{z}_{\mathrm{sc}})$, $\boldsymbol{e}_0^{\mathrm{s}}$, $\boldsymbol{e}_0^{\mathrm{u}}$ and $\boldsymbol{e}_0^{\pm c}$ are the associated eigenvectors for λ_{s}, λ_{u} and $\pm i\omega$ with unit moduli such that $\mathrm{Re}(\boldsymbol{e}_0^{+c}) = \mathrm{Re}(\boldsymbol{e}_0^{-c})$, and $\epsilon_c > 0$ and $T_{\mathrm{u,s}}$ are small constants. Equations (4.30) and (4.31) represent solutions of (4.28) such that $\boldsymbol{z}^{\mathrm{u}}(t) \to \bar{\boldsymbol{z}}(t)$ as $t \to -\infty$ and $\boldsymbol{z}^{\mathrm{s}}(t) \to \bar{\boldsymbol{z}}(t)$ as $t \to \infty$, as well as Eq. (4.29) represents a small periodic solution of (4.28) near $\boldsymbol{z}_{\mathrm{sc}}$. Note that $\bar{T} = 2\pi/\omega$ and $\lambda_s = -\lambda_u$ since the system (4.22) is Hamiltonian. The values of $\epsilon_c = 10^{-6}$, $\epsilon_{\mathrm{u,s}} = 10^{-4}$ and $T_{\mathrm{u,s}} = 10^{-2}$ are typically chosen in our numerical computations.

5 Detection of chaos in $\mathbb{P}_6(\pi_e)$

We apply the analytical and numerical techniques of §4 to $\mathbb{P}_6(\pi_e)$. As stated at the ends of §2, $\mathbb{P}_6(\pi_e)$ has the invariant plane $\mathbb{P}_6(\sigma_3\pi_e)$, on which there exist saddle-centers connected by homo- and/or heteroclinic orbits, as seen below.

We first introduce the following new symplectic transformation so that assumption (A1) holds and the $\boldsymbol{x}$-plane is invariant under the flow of (4.1):

$$x_1 = Q_3, \quad x_2 = P_3 - \frac{1}{2}P_4, \quad y_1 = Q_3 + 2Q_4 - \pi, \quad y_2 = \frac{1}{2}P_4. \tag{5.1}$$

Under the above transformation (5.1), the Hamiltonian (3.16) with $n = 1$ be-

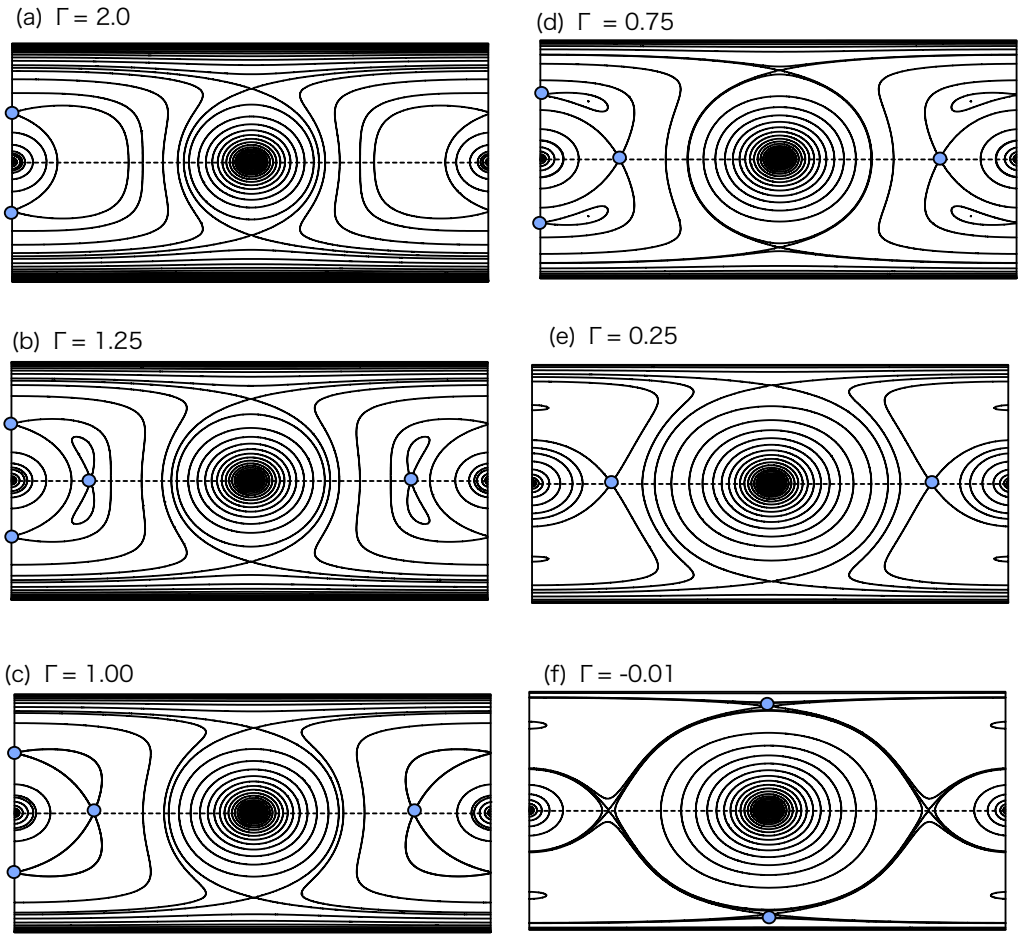

Figure 2: Phase portraits of (4.2) for $\mathbb{P}_6(\pi_e)$. The positions of saddle-centers are plotted as the filled circles $\bullet$.

comes

$$
\begin{aligned}
H(\boldsymbol{x},\boldsymbol{y}) = &-\frac{1}{2\pi}\log\left[1-\sqrt{1-(x_2+y_2)^2}\,\sin\frac{1}{2}(x_1+y_1)\right]\\
&-\frac{1}{2\pi}\log\left[1+\sqrt{1-(x_2+y_2)^2}\,\sin\frac{1}{2}(x_1+y_1)\right]\\
&-\frac{1}{2\pi}\log\left[1-\sqrt{1-(x_2-y_2)^2}\,\sin\frac{1}{2}(x_1-y_1)\right]\\
&-\frac{1}{2\pi}\log\left[1+\sqrt{1-(x_2-y_2)^2}\,\sin\frac{1}{2}(x_1-y_1)\right]\\
&-\frac{1}{2\pi}\log\left[1+(x_2^2-y_2^2)-\sqrt{(1-(x_2+y_2)^2)(1-(x_2-y_2)^2)}\,\cos x_1\right]\\
&-\frac{1}{2\pi}\log\left[1-(x_2^2-y_2^2)+\sqrt{(1-(x_2+y_2)^2)(1-(x_2-y_2)^2)}\,\cos y_1\right]\\
&-\frac{1}{4\pi}\log\left[1+(x_2+y_2)^2+(1-(x_2+y_2)^2)\,\cos(x_1+y_1)\right]\\
&-\frac{1}{4\pi}\log\left[1+(x_2-y_2)^2+(1-(x_2-y_2)^2)\,\cos(x_1-y_1)\right]\\
&-\frac{\Gamma}{2\pi}\log[(1-(x_2-y_2)^2)(1-(x_2+y_2)^2)]. \qquad (5.2)
\end{aligned}
$$

On the $\boldsymbol{x}$-plane the Hamiltonian (5.2) becomes

$$
\begin{aligned}
&H(\boldsymbol{x},\boldsymbol{0})\\
&=-\frac{1}{\pi}\log\left(1-\sqrt{1-x_2^2}\,\sin\frac{x_1}{2}\right)-\frac{1}{\pi}\log\left(1+\sqrt{1-x_2^2}\,\sin\frac{x_1}{2}\right)\\
&\quad-\frac{1}{2\pi}\log\left(1+x_2^2-(1-x_2^2)\cos x_1\right)-\frac{1}{2\pi}\log\left(1+x_2^2+(1-x_2^2)\cos x_1\right)\\
&\quad-\frac{1}{2\pi}\log 2(1-x_2^2)-\frac{\Gamma}{\pi}\log(1-x_2^2),
\end{aligned}
$$

and the $\boldsymbol{x}$-component system (4.2) has hyperbolic saddles

(i) at $\boldsymbol{s}_1=(\frac{1}{3}\pi,0)$ and $\boldsymbol{s}_2=(\frac{5}{3}\pi,0)$ for $\Gamma<\frac{3}{2}$;

(ii) at $\boldsymbol{s}_3=\left(\pi,\sqrt{\dfrac{3}{2(\Gamma+2)}}\right)$ and $\boldsymbol{s}_4=\left(\pi,-\sqrt{\dfrac{3}{2(\Gamma+2)}}\right)$ for $\Gamma>-\frac{1}{2}$;

(iii) at $\boldsymbol{s}_5=\left(0,\sqrt{\dfrac{1}{2(\Gamma+1)}}\right)$ and $\boldsymbol{s}_6=\left(0,-\sqrt{\dfrac{1}{2(\Gamma+1)}}\right)$ for $\Gamma>\frac{1}{2}$.

These hyperbolic saddles correspond to equilibria in (4.1) and have homo- or heteroclinic orbits. The phase portraits of (4.2) are displayed in Fig. 2 for several values of Γ. They also indicate the dynamics on the invariant plane $\mathbb{P}_6(\sigma_3\pi_e)$. As required in assumptions (A2) and (A2'), these equilibria are saddle-centers in (4.1)

(i') when $0<\Gamma<\frac{3}{2}$ for $\boldsymbol{s}_1$ and $\boldsymbol{s}_2$;

(ii') when $-\frac{1}{4}(5-\sqrt{15})(=-0.28175\ldots)<\Gamma<0$ for $\boldsymbol{s}_3$ and $\boldsymbol{s}_4$;

(iii') when $\Gamma>\frac{1}{2}$ for $\boldsymbol{s}_5$ and $\boldsymbol{s}_6$.

Finally, we see that assumption (A3) or (A3') holds as follows:

(ia') For $1<\Gamma<\frac{3}{2}$ there are a pair of homoclinic orbits to each of $\boldsymbol{s}_1$ and $\boldsymbol{s}_2$;

(ib') for $0<\Gamma<1$ there are two heteroclinic cycles between $\boldsymbol{s}_1$ and $\boldsymbol{s}_2$;

(ii') for $-\frac{1}{4}(5-\sqrt{15})<\Gamma<0$ there are a pair of homoclinic orbits to each of $\boldsymbol{s}_3$ and $\boldsymbol{s}_4$;

(iiia') for $\Gamma>1$ there are two heteroclinic cycles between $\boldsymbol{s}_5$ and $\boldsymbol{s}_6$;

(iiib') for $\frac{1}{2}<\Gamma<1$ there are a pair of homoclinic orbits to each of $\boldsymbol{s}_5$ and $\boldsymbol{s}_6$;

(iv') for $\Gamma=1$ there are four heteroclinic cycles between $\boldsymbol{s}_1$ or $\boldsymbol{s}_2$ and $\boldsymbol{s}_5$ or $\boldsymbol{s}_6$.

We give a summary of this statement in Table 1.

Table 1: Homoclinic or heteroclinic connections between saddle-centers on the $\boldsymbol{x}$-plane in $\mathbb{P}_6(\pi_e)$. The symbol $\boldsymbol{s}_p \leftrightarrow \boldsymbol{s}_q$ indicates that $\boldsymbol{s}_p$ and $\boldsymbol{s}_q$ have a heteroclinic ($p \neq q$) or a homoclinic ($p = q$) connection.

	Γ	homo- or heteroclinic connections	Fig. 2
ia'	$1 < \Gamma < \frac{3}{2}$	$\boldsymbol{s}_1 \leftrightarrow \boldsymbol{s}_1$, $\boldsymbol{s}_2 \leftrightarrow \boldsymbol{s}_2$	(b)
ib'	$0 < \Gamma < 1$	$\boldsymbol{s}_1 \leftrightarrow \boldsymbol{s}_2$	(d), (e)
ii'	$-\frac{1}{4}(5-\sqrt{15}) < \Gamma < 0$	$\boldsymbol{s}_3 \leftrightarrow \boldsymbol{s}_3$, $\boldsymbol{s}_4 \leftrightarrow \boldsymbol{s}_4$	(f)
iiia'	$\Gamma > 1$	$\boldsymbol{s}_5 \leftrightarrow \boldsymbol{s}_6$	(a), (b)
iiib'	$\frac{1}{2} < \Gamma < 1$	$\boldsymbol{s}_5 \leftrightarrow \boldsymbol{s}_5$, $\boldsymbol{s}_6 \leftrightarrow \boldsymbol{s}_6$	(d)
iv'	$\Gamma = 1$	$\boldsymbol{s}_1 \leftrightarrow \boldsymbol{s}_5$, $\boldsymbol{s}_1 \leftrightarrow \boldsymbol{s}_6$ $\boldsymbol{s}_2 \leftrightarrow \boldsymbol{s}_5$, $\boldsymbol{s}_2 \leftrightarrow \boldsymbol{s}_6$	(c)

For each of these cases we apply the numerical method of §4.2 to compute the conditions (4.20) and (4.21). First, we have each component of the second derivative $\mathrm{D}_y^2 H(\boldsymbol{x}, \boldsymbol{0})$ as

$$\frac{\partial^2 H}{\partial y_1^2}(\boldsymbol{x}, \boldsymbol{0}) = \frac{15x_2^4 - 22x_2^2 + 15 + 16(1-x_2^4)\cos x_1 + (1-x_2^2)^2 \cos 2x_1}{8\pi(1 + x_2^2 + (1-x_2^2)\cos x_1)^2},$$
$$\frac{\partial^2 H}{\partial y_1 \partial y_2}(\boldsymbol{x}, \boldsymbol{0}) = -\frac{6x_2 \sin x_1}{\pi(1 + x_2^2 + (1-x_2^2)\cos x_1)^2},$$
$$\frac{\partial^2 H}{\partial y_2^2}(\boldsymbol{x}, \boldsymbol{0}) = \frac{\mu_0(x_2) + \mu_1(x_2)\cos x_1 + \mu_2(x_2)\cos 2x_1 + \mu_3(x_2)\cos 3x_1}{4\pi(1-x_2^2)^2(1 + x_2^2 - (1-x_2^2)\cos x_1)(1 + x_2^2 + (1-x_2^2)\cos x_1)^2},$$

where

$$\begin{aligned}
\mu_0(x_2) =& 2[(2\Gamma+5)x_2^8 + (16\Gamma+9)x_2^6 + (28\Gamma-11)x_2^4 + (16\Gamma+15)x_2^2 + 2(\Gamma-1)],\\
\mu_1(x_2) =& (1 - x2^2)[(2\Gamma+5)x_2^6 + 6(5\Gamma+7)x_2^4 + (30\Gamma-67)x_2^2 + 2(\Gamma+2)],\\
\mu_2(x_2) =& -2(1-x_2^2)^2[(2\Gamma+5)x_2^4 + (4\Gamma-5)x_2^2 + 2(\Gamma-1)],\\
\mu_3(x_2) =& -(1-x_2^2)^3[(2\Gamma+5)x_2^2 + 2(\Gamma+2)].
\end{aligned}$$

At $\boldsymbol{x} = \boldsymbol{s}_j$ for $j = 1, 2, \ldots, 6$, the matrix $\mathrm{D}_y^2 H(\boldsymbol{x}, \boldsymbol{0})$ is diagonal and has the form of (4.11) with

$$m_1 = \frac{5}{4\pi}, \quad m_2 = \frac{2\Gamma}{\pi},$$

for $\boldsymbol{x} = \boldsymbol{s}_1, \boldsymbol{s}_2$;

$$m_1 = -\frac{\Gamma}{2\pi}, \quad m_2 = \frac{2(\Gamma+2)(8\Gamma^2+20\Gamma+5)}{\pi(2\Gamma+1)^2},$$

for $\boldsymbol{x} = \boldsymbol{s}_3, \boldsymbol{s}_4$; and

$$m_1 = \frac{8\Gamma+5}{8\pi(\Gamma+1)}, \quad m_2 = \frac{8\Gamma(\Gamma+1)^2}{\pi(2\Gamma+1)^2},$$

for $\boldsymbol{x} = \boldsymbol{s}_5, \boldsymbol{s}_6$. To obtain a starting solution for the boundary value problem (4.2), (4.4), (4.16) and (4.17), we use a Fortran code called "DOP853" [10] to

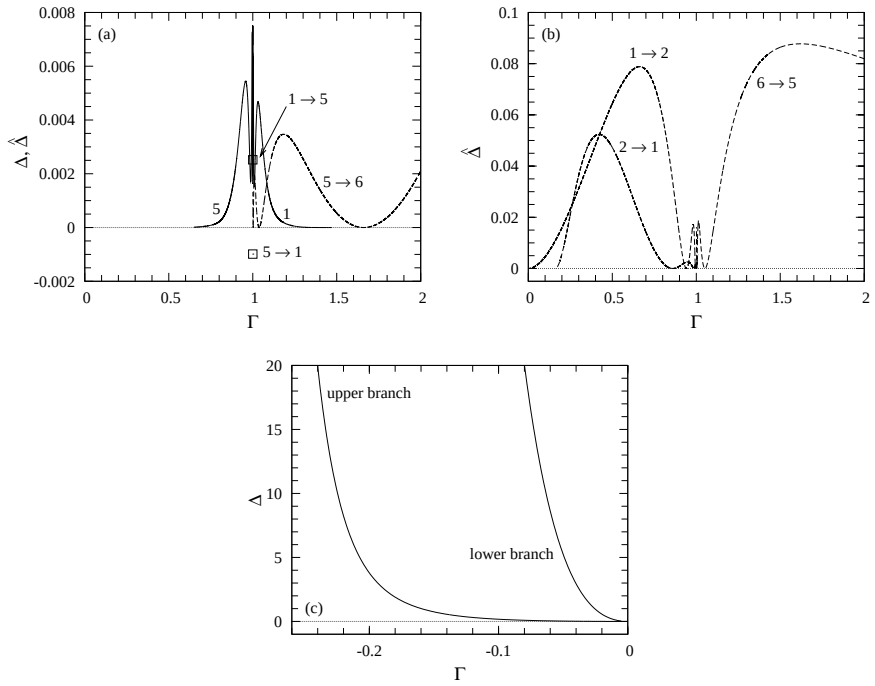

Figure 3: Computational results of Δ and $\hat{\Delta}$: (a) Homo- and heteroclinic orbits to $\boldsymbol{s}_{1,5,6}$; (b) heteroclinic orbits to $\boldsymbol{s}_{1,2,5,6}$; (c) upper and lower homoclinic orbits to $\boldsymbol{s}_3$. Δ is plotted as solid lines, while $\hat{\Delta}$ is plotted as dotted lines or "□". The labels represent the subscripts of equilibria which the associated homo- or heteroclinic orbit connect. Note that Δ has the same value for homoclinic orbits to $\boldsymbol{s}_{2k}$ and $\boldsymbol{s}_{2k-1}$ and $\hat{\Delta}$ has the same positive (resp. negative) value for heteroclinic orbits from $\boldsymbol{s}_1$ or $\boldsymbol{s}_2$ to $\boldsymbol{s}_5$ or $\boldsymbol{s}_6$ and (resp. from $\boldsymbol{s}_5$ or $\boldsymbol{s}_6$ to $\boldsymbol{s}_1$ or $\boldsymbol{s}_2$).

solve (4.2) and (4.4) as an initial value problem as stated at the end of §4.2. The code is based on the explicit Runge-Kutta method of order 8 by Dormand and Prince [7], and a fifth order error estimator with third order correction is utilized. It also has a dense output of order 7. See [10] for more details on the code. A small tolerance of 10^{-8} or 10^{-9} is chosen in the computations so that the numerical results are very accurate. For instance, the value of the Hamiltonian energy changes by only 10^{-15} at most for the numerical solutions.

Figure 3 shows the computational results of Δ and $\hat{\Delta}$. We see that Δ and $\hat{\Delta}$ are positive for except $\Gamma = 1$. Hence, by Theorems 4.1 and 4.2, there exist transverse homoclinic orbits to periodic orbits near the saddle-centers and chaotic dynamics occurs for $\Gamma \neq 1$. On the other hand, $\hat{\Delta}$ is negative for a heteroclinic orbit connecting $\boldsymbol{s}_5$ to $\boldsymbol{s}_1$ at $\Gamma = 1$, which means that the unstable manifold of periodic orbits near the saddle-center $(\boldsymbol{s}_1, \boldsymbol{0})$ does not intersect the stable manifold of periodic orbits near $(\boldsymbol{s}_5, \boldsymbol{0})$. Thus, the Melnikov theory says nothing about the occurrence of chaos for $\Gamma = 1$.

To demonstrate the theoretical results above, we compute the stable and

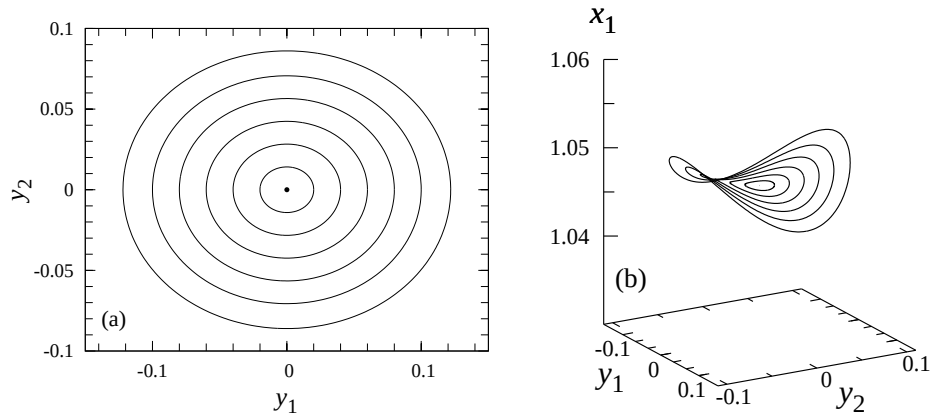

Figure 4: Periodic orbits near the saddle-center $(s_1, 0)$ for $\Gamma = 1.25$: (a) Their projections to the $\boldsymbol{y}$-plane; (b) to the (y_1, y_2, x_1)-space. The outmost periodic orbit has Hamiltonian energy of $H = 0.03$.

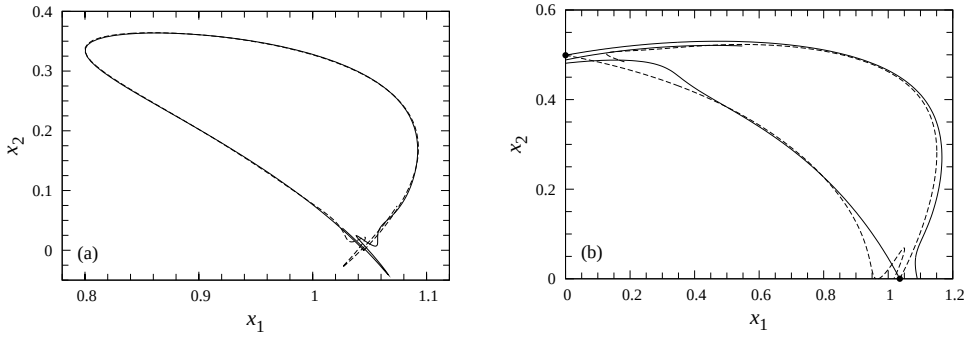

Figure 5: Stable and unstable manifolds of periodic orbits on the Poincaré section $\{y_2 = 0\}$: (a) For a periodic orbit near $(\boldsymbol{s}_1, \boldsymbol{0})$ for $\Gamma = 1.25$ and $H = 0.03$; (b) for periodic orbits near $(\boldsymbol{s}_1, \boldsymbol{0})$ and $(\boldsymbol{s}_5, \boldsymbol{0})$ for $\Gamma = 1$ and $H = 0.04$. The solid and broken lines represent the stable and unstable manifolds, respectively. In plate (b) the point "$\bullet$" represents the periodic orbits on the Poincaré section.

unstable manifolds of periodic orbits near saddle-centers with the numerical method of §4.3. Figures 4 and 5, respectively, show periodic orbits near the saddle-center $(\boldsymbol{s}_1, \boldsymbol{0})$ for $\Gamma = 1.25$, and the stable and unstable manifolds of periodic orbits on the Poincaré section, $\{(\boldsymbol{x}, \boldsymbol{y}) \in \mathbb{R}^2 \times \mathbb{R}^2 \,|\, y_2 = 0\}$, for $\Gamma = 1.25$ and 1. In Fig. 5(a), the stable and unstable manifolds of the outmost periodic orbit in Fig. 4 intersect transversely. In Fig. 5(b), the stable and unstable manifolds of periodic orbits near $(\boldsymbol{s}_1, \boldsymbol{0})$ and $(\boldsymbol{s}_5, \boldsymbol{0})$ are displayed when the saddle-centers have heteroclnic connections at $\Gamma = 1$ (see Fig. 2(c)). We see that the unstable (resp. stable) manifold of the periodic orbit near $(\boldsymbol{s}_1, \boldsymbol{0})$ intersects transversely (resp. does not intersect) the stable (resp. unstable) manifold of periodic orbit near $(\boldsymbol{s}_5, \boldsymbol{0})$, as our theory predicts. However, since

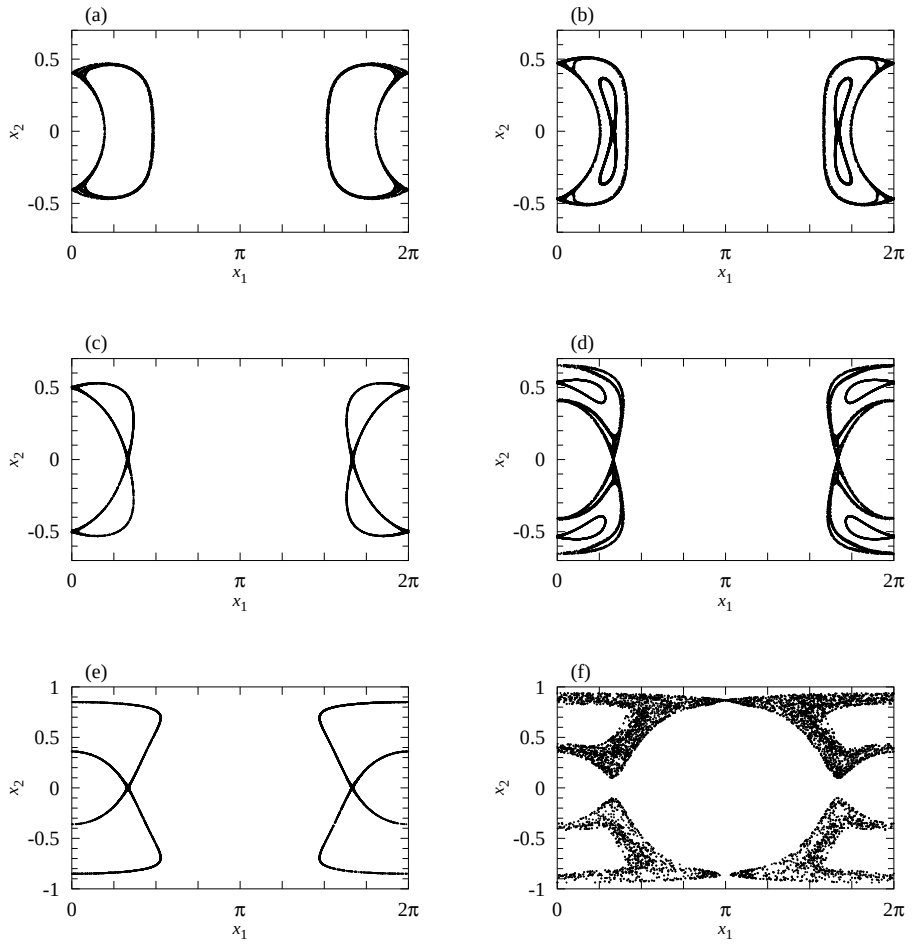

Figure 6: Poincaré sections ($y_2 = 0$, $\dot{y}_2 > 0$) for chaotic motions obtained by direct numerical simulation: (a) $\Gamma = 2$ and $H = 0.0995$; (b) $\Gamma = 1.25$ and $H = 0.03$ or 0.0485 (near homoclinic orbits to $\boldsymbol{s}_{1,2}$ or heteroclinic orbits to $\boldsymbol{s}_{5,6}$); (c) $\Gamma = 1$ and $H = 0.0275$; (d) $\Gamma = 0.75$ and $H = 0.0270425$ or 0.003 (near heteroclinic orbits to $\boldsymbol{s}_{1,2}$ or homoclinic orbits to $\boldsymbol{s}_{5,6}$); (e) $\Gamma = 0.25$ and $H = 0.0273$; (f) $\Gamma = -0.01$ and $H = -0.0621567265$.

the stable and unstable manifolds of the periodic orbit near $(\boldsymbol{s}_1, \boldsymbol{0})$ intersect transversely as observed in Fig. 5(b), chaotic dynamics also occurs for $\Gamma = 1$.

Finally, we give some direct numerical simulations for chaotic motions near the saddle-center. Figure 6 shows projections onto the $\boldsymbol{x}$-plane of trajectories on the Poincaré section $\{y_2 = 0\}$ with initial points near the saddle-centers. To obtain the cross section points from the trajectories, an interval $[t_{n-1}, t_n]$ of numerical integration such that $y_2(t_{n-1}) < 0$ and $y_2(t_n) \geq 0$ is searched and the secant method is applied to the dense output for the interval with a tolerance of $|y_2| < 10^{-8}$. All these computations are performed by a software called "Dynamics" [16] into which the C version of the code "DOP853" [10] is

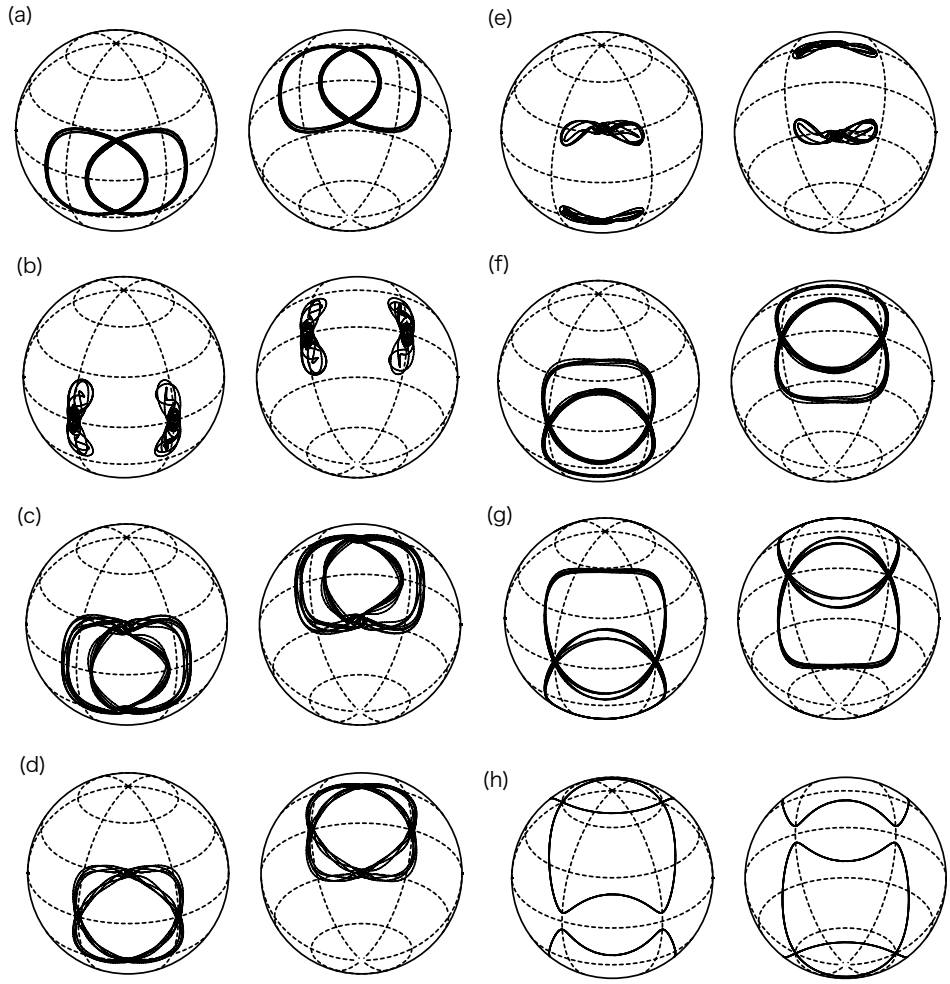

Figure 7: Chaotic orbits near homo- or heteroclinic orbits to the saddle-centers, each of which corresponds to the Poincaré map in Figure 6: (a) $\boldsymbol{s}_5$ for $\Gamma = 2$; (b) $\boldsymbol{s}_1$ for $\Gamma = 1.25$; (c) $\boldsymbol{s}_5$ for $\Gamma = 1.25$; (d) $\boldsymbol{s}_1$ and s_5 for $\Gamma = 1$; (e) $\boldsymbol{s}_5$ for $\Gamma = 0.75$; (f) $\boldsymbol{s}_1$ for $\Gamma = 0.75$; (g) $\boldsymbol{s}_1$ for $\Gamma = 0.25$; (h) $\boldsymbol{s}_3$ for $\Gamma = -0.01$. Note that the first and the fourth point vortices stay at the equator due to (2.15).

built in a manner explained in [29]. We also show actual chaotic orbits near the 6-ring on the sphere in Fig. 7, which correspond to the Poincaré sections in Fig. 6. Both of them clearly illustrate chaotic behavior near the homo- or heteroclinic orbits to the saddle-centers.

6 Detection of chaos in $\mathbb{P}_5(\pi_o)$

For $\mathbb{P}_5(\pi_o)$, as stated in §3.2, the analytic technique of §4.1 is not applicable since it has no invariant plane. Thus, applying only the numerical approach of §4.3, we compute the stable and unstable manifolds of periodic orbits near the saddle-center and detect the occurrence of chaos.

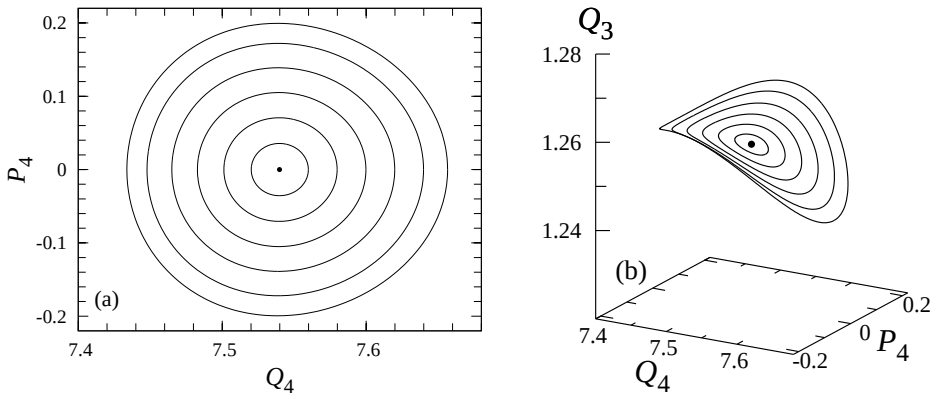

Figure 8: Periodic orbits near the saddle-center $(Q_3, Q_4, P_3, P_4) = (2\pi/5, 12\pi/5, 0, 0)$ for $\Gamma = 0.5$: (a) Their projections onto the (Q_4, P_4)-plane; (b) onto the (Q_4, P_4, Q_3)-space.

The Hamiltonian (3.19) with $n = 1$ has an equilibrium at $(Q_3, Q_4, P_3, P_4) = (2\pi/5, 12\pi/5, 0, 0)$, which corresponds to the 5-ring at the equator

$$\boldsymbol{X}_0 = \left(\frac{\pi}{2}, \frac{\pi}{2}, \frac{\pi}{2}, \frac{\pi}{2}, \frac{\pi}{2}, 0, \frac{2}{5}\pi, \frac{4}{5}\pi, -\frac{4}{5}\pi, -\frac{2}{5}\pi\right),$$

as in Proposition 2.2. It becomes a saddle-center equilibrium for $0 < \Gamma < 1$, since the Hessian of the Hamiltonian $H_1^{(5)}$ at this point has the eigenvalues

$$\pm\frac{\sqrt{83 + 15\sqrt{5} - 150\Gamma - \sqrt{\left(83 + 15\sqrt{5}\right)^2 + 300\Gamma(-51 - 15\sqrt{5} + 43\Gamma)}}}{4\sqrt{5}\pi},$$

which are purely imaginary for $\Gamma > 0$ and real for $\Gamma < 0$, and

$$\pm\frac{\sqrt{83 + 15\sqrt{5} - 150\Gamma + \sqrt{\left(83 + 15\sqrt{5}\right)^2 + 300\Gamma(-51 - 15\sqrt{5} + 43\Gamma)}}}{4\sqrt{5}\pi},$$

which are purely imaginary for $\Gamma > 1$ and real for $\Gamma < 1$.

Figure 8 shows periodic orbits near the saddle-center for $\Gamma = 0.5$, and Figure 9 shows the stable and unstable manifolds of the outmost periodic orbit in Fig. 8 on the Poincaré section $\{P_4 = 0\}$. Compared with the results of $\mathbb{P}_6(\pi_e)$ in §5, the behavior of the invariant manifolds is very complicated. This is due to the fact that there is no invariant plane having a homoclinic orbit in $\mathbb{P}_5(\pi_o)$. Nevertheless, we see that they really intersect transversely (without self-intersections) and hence chaotic dynamics occurs. Figure 10 shows the Poincaré section $\{P_4 = 0\}$ for a trajectory with an initial point near the saddle-center and its corresponding orbit of the 5-ring on the sphere, which clearly demonstrate chaotic behavior.

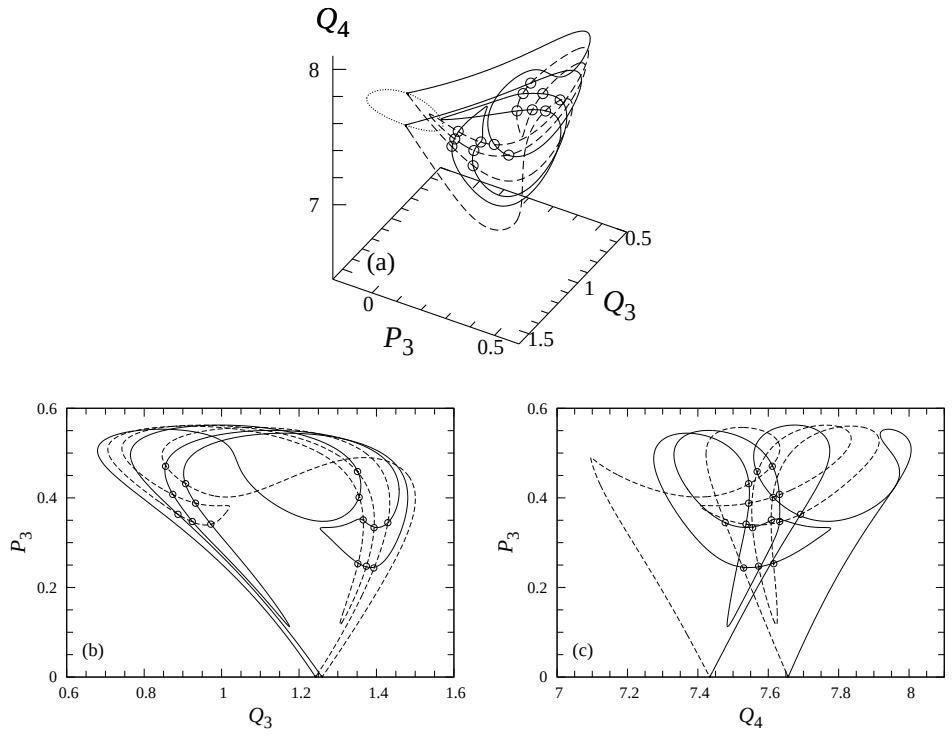

Figure 9: Stable and unstable manifolds of a periodic orbit on the Poincaré section $\{P_4 = 0\}$ for $\Gamma = 0.5$ and $H = -0.087$; (a) In the (Q_3, P_3, Q_4)-space; (b) their projections onto the (Q_3, P_3)-plane; (c) onto the (Q_4, P_3)-plane. The solid and broken lines represent the stable and unstable manifolds, respectively, and the circle "$\circ$" represents homoclinic points. The dotted lines represents the projection of the periodic orbit (not on the Poincaré section) onto the (Q_3, P_3, Q_4)-space in plate (a).

7 Summary and discussion

We have shown the existence of chaotic motions in two-degree-of-freedom Hamiltonian systems with saddle-center equilibria derived from the N-vortex problem on the sphere according to the reduction method of [22]. Utilizing the analytical and numerical techniques proposed in [27, 29, 30, 31] for $N = 6$, we numerically proved that the stable and unstable manifolds of periodic orbits around saddle-center equilibria intersect transversely and hence chaotic orbits exist. We also have numerically shown that the unstable and stable manifolds of the periodic orbits near the saddle-center intersects transversely and given some direct numerical results to illustrate the existence of chaotic orbits near the saddle-centers for $N = 5$ and 6.

The analytical and numerical approaches we used depend on the structure of the reduced four-dimensional system: For $N = 6n$, we make the best use of the Melnikov-type analysis[27] since the reduced system satisfies a key assumption in the analysis, i.e., it contains a two-dimensional invariant plane consisting of

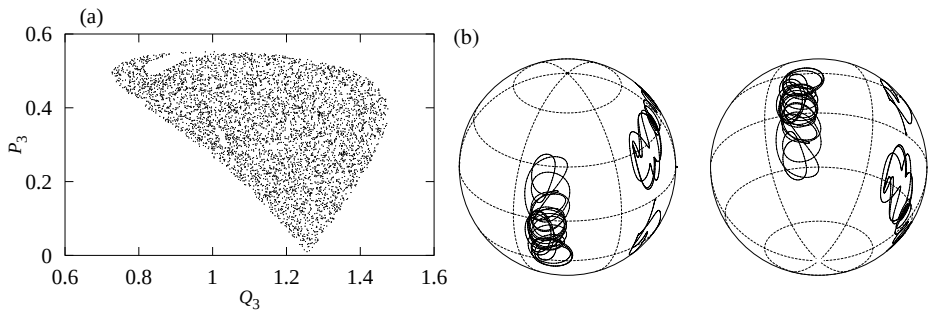

Figure 10: (a) Poincaré section $P_4 = 0$ for a chaotic motion with an initial point near $(Q_3, Q_4, P_3, P_4) = (2/5\pi, 12/5\pi, 0, 0)$ for $\Gamma = 0.5$; (b) its corresponding chaotic orbit near the 5-ring on the sphere. We see the only four trajectories on the sphere, since the first point vortex in $\mathbb{P}_5(\pi_o)$ is fixed at the equator due to (2.14).

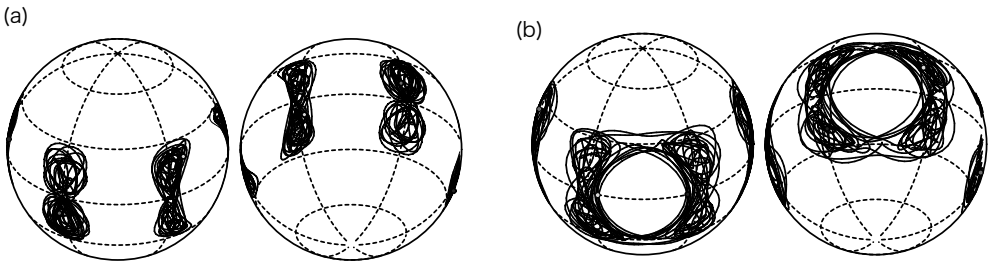

Figure 11: Chaotic orbits of the perturbed 6-ring in the full 6-vortex problem (1.1) and (1.2) up to $t = 500$ in the presence of the identical pole vortices: (a) $\Gamma = 1.25$; (b) $\Gamma = 1.00$; (c) $\Gamma = 0.75$; and (d) $\Gamma = 0.25$.

the stable and unstable eigenspaces. On the other hand, the Melnikov analysis is not applicable for $N = 5n$ since the reduced system has no such invariant plane. Thus we rely on the direct numerical computation of the unstable and the stable manifolds [31] to show their transverse intersection.

Finally, we discuss how chaotic orbits found in the reduced system appear in the full 6-vortex problem on the sphere. We first note that if the 6-ring corresponds to a saddle-center equilibrium in the reduced system $\mathbb{P}_6(\pi_e)$, then $(\lambda_1^{\pm})^2 < 0 < (\lambda_2^{\pm})^2$ and hence the maximum eigenvalue λ_3^+ becomes positive since $(\lambda_2^{\pm})^2 < (\lambda_3^{\pm})^2$. Thus, the eigenspace for λ_3^+, which is not included in the reduced system, give the most unstable directions, and inevitably affects the dynamics of the full system. However, we expect that solutions of the full system also exhibit chaotic motions since by the Poincaré recurrence theorem [1], they must repeatedly return in neighborhoods of chaotic orbits in the reduced system if they start there. Figure 11 shows numerical solutions of (1.1) and (1.2) with the identical pole vortices when the 6-ring is slightly perturbed. We see that chaotic motions occur in the full system, as we have expected. Moreover, for

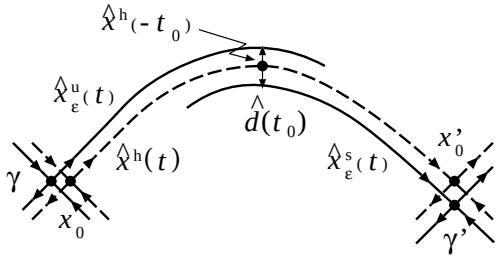

Figure A1: Orbits on the stable and unstable manifolds

$\Gamma = 1.25$ and 1, the chaotic orbits of Figs. 11(a) and (b) seem to evolve around those in the reduced systems in Figs. 7(b) and (d).

The Melnikov-type method was extended to three- or more-degree-of-freedom Hamiltonian systems with saddle-centers in [28]. The reduced systems $\mathbb{P}_N(\pi_o)$ and $\mathbb{P}_N(\pi_e)$ in (2.12) and (2.13) are multi-degree-of-freedom Hamiltonian and the N-ring corresponds to a saddle-center equilibrium for a certain range of Γ. So the reader may think that it is also applicable to the N vortex problem on the sphere but this is not the case. For instance, Proposition 2.3 shows that $\mathbb{P}_8(\pi_e)$ is a multi-degree-of-freedom Hamiltonian system in which the phase space is represented by

$$\boldsymbol{X} = \boldsymbol{X}_0 + \sum_{k=1}^{3} \left(b_k^+ \boldsymbol{\phi}_k^+ + b_k^- \boldsymbol{\phi}_k^- \right), \quad b_k^\pm \in \mathbb{R},$$

where $\boldsymbol{X}_0$ represents the 8-ring at the equator. The 8-ring becomes a saddle-center equilibrium when the eigenvalues λ_3^+ and λ_3^- are positive and negative, respectively, and the other eigenvalues $\lambda_2^\pm$ and $\lambda_1^\pm$ are purely imaginary, but the eigenspace spanned by the eigenvectors for $\lambda_3^\pm$ is not invariant for $\mathbb{P}_8(\pi_e)$. (See the list of invariant dynamical systems in $\mathbb{P}_8$ in [23].) Thus the Melnikov-type method of [28] is not applicable. However, the numerical approach given in §4.3 is still available and numerical results in this direction will be reported in the near future.

A Proof of Theorem 4.2

We outline the proof of Theorem 4.2, which is very similar to that of Theorem 1.1 of [27].

Let $\hat{\boldsymbol{z}}^{\rm u}_\epsilon(t;t_0) = (\hat{\boldsymbol{x}}^{\rm u}_\epsilon(t;t_0), \hat{\boldsymbol{y}}^{\rm u}_\epsilon(t;t_0))$ and $\hat{\boldsymbol{z}}^{\rm s}_\epsilon(t;t_0) = (\hat{\boldsymbol{x}}^{\rm s}_\epsilon(t;t_0), \hat{\boldsymbol{y}}^{\rm s}_\epsilon(t;t_0))$ be orbits on the unstable manifold of a periodic orbit γ near the saddle-center $(\boldsymbol{x}'_0, \boldsymbol{0})$ and on the stable manifold of a periodic orbit γ' near the saddle-center $(\boldsymbol{x}_0, \boldsymbol{0})$, respectively, such that they pass near $(\boldsymbol{x}, \boldsymbol{y}) = (\hat{\boldsymbol{x}}^{\rm h}(-t_0), \boldsymbol{0})$ and the distances between γ and $(\boldsymbol{x}_0, \boldsymbol{0})$ and between γ' and $(\boldsymbol{x}'_0, \boldsymbol{0})$ are $O(\epsilon)$, where ϵ is a constant such that $0 < \epsilon \ll 1$. See Fig. A1. As in Lemma 3.2 of [27], we can represent the orbits $\boldsymbol{z}^{\rm s,u}_\epsilon(t;t_0)$ as

$$\hat{\boldsymbol{x}}^{\rm u}_\epsilon(t;t_0) = \hat{\boldsymbol{x}}^{\rm h}(t-t_0) + O(\epsilon^2), \quad \hat{\boldsymbol{y}}^{\rm u}_\epsilon(t;t_0) = \epsilon \hat{\Psi}(t-t_0) \hat{B}_-^{-1} \Phi(t_0) \boldsymbol{\eta}_0 \qquad \text{(A.1)}$$

for $t \in [-t_2, 0]$ and

$$\hat{\boldsymbol{x}}^{\rm s}_\epsilon(t;t_0) = \hat{\boldsymbol{x}}^{\rm h}(t-t_0) + O(\epsilon^2), \quad \hat{\boldsymbol{y}}^{\rm s}_\epsilon(t;t_0) = \epsilon\hat{\Psi}(t-t_0)\hat{B}_+^{-1}\hat{\Phi}(t_0)\boldsymbol{\eta}_0 \tag{A.2}$$

for $t \in [0, t_1]$, where t_1 and t_2 are any positive numbers. Let $d(t_0;\boldsymbol{\eta}_0,\epsilon)$ be the distance between the orbits $\hat{\boldsymbol{z}}^{\rm s,u}_\epsilon(t;t_0)$ along the direction $({\rm D}_x H(\hat{\boldsymbol{x}}^{\rm h}(-t_0),\boldsymbol{0}),\boldsymbol{0})$ at $t=0$ (see Fig. A1). Using an argument given in §3 of [27], we can show that

$$\frac{1}{\epsilon^2} d(t_0;\boldsymbol{\eta}_0,\epsilon) = \frac{\tilde{M}(t_0)}{|{\rm D}_x H(\hat{\boldsymbol{x}}^{\rm h}(-t_0),\boldsymbol{0})|} + O(\epsilon), \tag{A.3}$$

where

$$\tilde{M}(t_0) = \int_{-\infty}^{\infty} {\rm D}_x H(\hat{\boldsymbol{x}}^{\rm h}(t),\boldsymbol{0}) \cdot \boldsymbol{g}(\hat{\boldsymbol{x}}^{\rm h}(t), \hat{\Psi}(t)\hat{B}_-^{-1}\Phi(t_0)\boldsymbol{\eta}_0){\rm d}t \tag{A.4}$$

with

$$\boldsymbol{g}(\boldsymbol{x},\boldsymbol{\eta}) = \frac{1}{2}{\rm D}_y^2 \boldsymbol{f}(\boldsymbol{x},\boldsymbol{0})(\boldsymbol{\eta},\boldsymbol{\eta}), \quad \boldsymbol{f}(\boldsymbol{x},\boldsymbol{y}) = J_1 {\rm D}_x H(\boldsymbol{x},\boldsymbol{y}).$$

We easily prove the following lemma like Lemmas 3.3 of [27].

Lemma A.1. *For any $\boldsymbol{\eta}_0, \boldsymbol{\eta}_0' (\neq 0) \in \mathbb{R}^2$ and $t_0' \in \mathbb{R}$, there exist real numbers ρ, t_0 such that*

$$\tilde{M}(t_0';\boldsymbol{\eta}_0') = \rho^2 \tilde{M}(t_0;\boldsymbol{\eta}_0).$$

Let $\boldsymbol{\eta}(t) = \hat{\Psi}(t)\hat{\boldsymbol{\eta}}_0$ for any $\hat{\boldsymbol{\eta}}_0 \in \mathbb{R}^2$. As in the proof of Lemmas 3.4 of [27], we have

$$\frac{\rm d}{{\rm d}t}[{\rm D}_y^2 H(\boldsymbol{x}^{\rm h}(t),\boldsymbol{0})(\boldsymbol{\eta}(t),\boldsymbol{\eta}(t))] = -2{\rm D}_x H(\boldsymbol{x}^{\rm h}(t),\boldsymbol{0}) \cdot \boldsymbol{g}(\boldsymbol{x}^{\rm h}(t),\boldsymbol{\eta}(t)). \tag{A.5}$$

Hence

$$\int_{-\infty}^{\infty} {\rm D}_x H(\hat{\boldsymbol{x}}^{\rm h}(t),\boldsymbol{0}) \cdot \boldsymbol{g}(\boldsymbol{x}^{\rm h}(t),\boldsymbol{\eta}(t)){\rm d}t = m(\boldsymbol{\eta}(-\infty)) - m'(\boldsymbol{\eta}(\infty)). \tag{A.6}$$

Substituting $\boldsymbol{\eta}(t) = \hat{\Psi}(t)\hat{B}_-^{-1}\Phi(t_0)\boldsymbol{\eta}_0$ into (A.6) and using (4.8), we prove the following lemma.

Lemma A.2. *We have*

$$\tilde{M}_1(t_0;\boldsymbol{\eta}_0) = m(\boldsymbol{\eta}_0) - m'(\hat{B}_0\Phi(t_0)\boldsymbol{\eta}_0). \tag{A.7}$$

In particular, for $\boldsymbol{e}_1 = (1,0)^{\rm T}$

$$\tilde{M}_1(t_0;\boldsymbol{e}_1) = \hat{M}(t_0).$$

From Lemmas A.1 and A.2 we see that if $\hat{M}(t_0)$ has a simple zero, then $\tilde{M}(t_0;\boldsymbol{\eta}_0)$ does so for any nonzero $\boldsymbol{\eta}_0 \in \mathbb{R}^2$. Applying the implicit function theorem to (A.3) at $\epsilon = 0$, we complete the proof of Theorem 4.2. □

Acknowledgments

This work is partially supported by Ministry of Education, Science, Sports and Culture, Grand-in-Aid for Young Scientists (A) #17684002, Grand-in-Aid for Exploratory #19654014, and Grand-in-Aid for formation of COE at Hokkaido University; and by the Japan Society for the Promotion of Science, Grant-in-Aid for Scientific Research (C) #18560056.

References

[1] V.I. Arnold, *Mathematical Methods of Classical Mechanics*, 2nd. ed. Springer-Verlag, New York, 1989.

[2] V.I. Arnold, *Ordinary Differential Equations*. Springer-Verlag, New York, 1992.

[3] S. Boatto and H.E. Cabral, *Nonlinear stability of a latitudinal ring of point-vortices on a nonrotating sphere*, SIAM J. Appl. Math., 64 (2003), pp. 216–230.

[4] H.E. Cabral, K.R. Meyer and D.S. Schmidt, *Stability and bifurcation of the $N+1$ vortex problem on sphere*, Regular Chaotic Dyn., 8 (2003) pp. 259–282.

[5] A.R. Champneys and G.J. Lord, *Computation of homoclinic solutions to periodic orbits in a reduced water-wave problem*, Physica D, 102 (1993), 232–269.

[6] E. Doedel, A.R. Champneys, T.F. Fairgrieve, Y.A. Kuznetsov, B. Sandstede and X. Wang, *AUTO97: Continuation and Bifurcation Software for Ordinary Differential Equations (with HomCont)*, 1997, available by anonymous ftp from `ftp.cs.concordia.ca`, directory `pub/doedel/auto`.

[7] J.R. Dormand and P.J. Prince, *Practical Runge-Kutta processes*, SIAM J. Sci. Stat. Comput. 10 (1989), pp. 977–989.

[8] D.G. Dritschel, *The stability and energetics of co-rotating uniform vortices*, J. Fluid Mech., 358 (1985), pp. 95–134.

[9] J. Guckenheimer and P. Holmes, *Nonlinear Oscillations, Dynamical Systems, and Bifurcations of Vector Fields*, Springer-Verlag, New York, 1983.

[10] E. Hairer, S.P. Nørsett, G. Wanner, *Solving Ordinary Differential Equations I*, 2nd ed., Springer-Verlag, Berlin, 1993.

[11] G. Haller, *Chaos Near Resonance*, Springer-Verlag, New York, 1999.

[12] R. Kidambi and P.K. Newton, *Collapse of three vortices on a sphere*, Nouvo Cimento, 22C (1999), pp. 779–791.

[13] L.G. Kurakin, *On nonlinear stability of the regular vortex systems on a sphere*, Chaos, 14 (2004), pp. 592–602.

[14] K.R. Meyer and G.R. Hall, *Introduction to Hamiltonian Dynamical Systems and the N-Body Problem*, Springer-Verlag, New York, 1992.

[15] P.K. Newton, *The N-vortex problem, Analytical techniques*, Springer-Verlag, New York, 2001.

[16] H.E. Nusse and J.A. Yorke, *Dynamics: Numerical Explorations*, 2nd ed., Springer-Verlag, New York, 1998.

[17] S. Pekarsky and J.E. Marsden, *Point vortices on a sphere: Stability of relative equilibria*, J. Math. Phys., 39 (1998), pp. 5894–5907.

[18] L.M. Polvani and D.G. Dritschel, *Wave and vortex dynamics on the surface of a sphere*, J. Fluid Mech., 255 (1993), pp. 35–64.

[19] T. Sakajo, *Motion of a vortex sheet on a sphere with pole vortices*, Phys. Fluids, 16 (2004), pp. 717–727.

[20] T. Sakajo, *Transition of global dynamics of a polygonal vortex ring on a sphere with pole vortices*, Physica D, 196 (2004), pp. 243–264.

[21] T. Sakajo, *High-dimensional heteroclinic and homoclinc connections in odd point-vortex ring on a sphere*, Nonlinearity, 19 (2005), pp. 75–93.

[22] T. Sakajo, *Invariant dynamical systems embedded in the N-vortex problem on a sphere with pole vortices*, Physica D, 217 (2006), pp. 142–152.

[23] T. Sakajo, *Erratum: Invariant dynamical systems embedded in the N-vortex problem on a sphere with pole vortices*, full system. Physica D, 225 (2007), pp. 235–236.

[24] S. Wiggins, *Global Bifurcations and Chaos*, Springer-Verlag, New York, 1988.

[25] S. Wiggins,*Global Dynamics, Phase Space Transport, Orbits Homoclinic to Resonances, and Applications*,American Mathematical Society, Providence, RI, 1993.

[26] S. Wiggins, *Introduction to Applied Nonlinear Dynamical Systems and Chaos*, 2nd ed., Springer-Verlag, 2003.

[27] K. Yagasaki, *Horseshoes in two-degree-of-freedom Hamiltonian systems with saddle-centers*, Arch. Rat. Mech. Anal., 154 (2000), pp. 275-296.

[28] K. Yagasaki, *Homoclinic and heteroclinic orbits to invariant tori in multi-degree-of-freedom Hamiltonian systems with saddle-centers*, Nonlinearity, 18 (2005), pp. 1331-1350.

[29] K. Yagasaki, *Numerical analysis for global bifurcations of periodic orbits in autonomous differential equations*, in preparation.

[30] K. Yagasaki, *Numerical computation of homoclinic and heteroclinic orbits to nonhyperbolic trajectories*, in preparation.

[31] K. Yagasaki, *Numerical computation of stable and unstable manifolds of normally hyperbolic invariant manifolds*, in preparation.